Dysfunctional Hippocampal-Prefrontal Network Underlies a Multidimensional Neuropsychiatric Phenotype following Early-Life Seizure

Running head: HPC-PFC dysfunction and early-life seizure

Rafael Naime Ruggiero[1*], Danilo Benette Marques[1#], Matheus Teixeira Rossignoli[1#], Jana Batista De Ross[1], Tamiris Prizon[1], Ikaro Jesus Silva Beraldo[2,3], Lezio Soares Bueno-Junior[4], Ludmyla Kandratavicius[5], Jose Eduardo Peixoto-Santos[6], Cleiton Lopes Aguiar[2,3], João Pereira Leite[1*].

[1]Department of Neuroscience and Behavioral Sciences, Ribeirão Preto Medical School, University of São Paulo, Ribeirão Preto, São Paulo, Brazil.
[2]Department of Physiology and Biophysics Federal University of Minas Gerais, Belo Horizonte, Minas Gerais, Brazil.
[3]Laboratory of Molecular and Behavioral Neuroscience (LANEC), Federal University of Minas Gerais, Belo Horizonte, Brazil
[4]Department of Psychiatry, University of Michigan Medical School, Ann Arbor, Michigan, USA
[5]Department of Pathology, State University of Campinas, Campinas, São Paulo, Brazil
[6]Neuroscience Discipline, Department of Neurology and Neurosurgery, Universidade Federal de São Paulo, São Paulo, Brazil

***Corresponding author:** rafaruggiero@gmail.com, jpleite@fmrp.usp.br
[#]DBM and MTR contributed equally to this work

Conflict of interest

The authors declare no competing financial interests.

Acknowledgements

This research was funded by Fundação de Amparo à Pesquisa do Estado de São Paulo - FAPESP (R.N.R.: 2018/02303-4; M.T.R.: 2020/01510-6; D.B.M.:

2022/16812-3; J.P.L.: 2016/17882-4), Coordenação de Aperfeiçoamento de Pessoal de Nível Superior - CAPES - Finance Code 001 (D.B.M.: 88882.328283/2019-01), and Conselho Nacional de Desenvolvimento Científico e Tecnológico - CNPq (J.P.L.: 305104/2020-9 and 422911/2021-6; T.P.: 164165/2018-5). We thank Renato Meirelles e Silva, Renata Caldo Scandiuzzi and Daniela Ribeiro for technical support. We thank Ana Carolina Medeiros and Rafael D'Agosta for helping with the photomicrography and histology. We also thank Patrick Forcelli, Claudio Queiroz, Marcelo Caetano, Tonicarlo Velasco, Ricardo Saute and Norberto Garcia Cairasco for discussions. RNR and JPL designed the research. RNR, CLA and LSBJ developed the methodology. RNR, DBM, TP and MTR conducted the experiments. RNR, DBM, and IJSB analyzed data. MTR edited the figures. JBDR, LK, TP and JEPS performed immunohistochemistry. TP and JEPS conducted the neurochemistry experiments. JPL supervised the project. All authors wrote and revised the manuscript.

Abstract

Brain disturbances during development can have a lasting impact on neural function and behavior. Seizures during this critical period are linked to significant long-term consequences such as neurodevelopmental disorders, cognitive impairments, and psychiatric symptoms, resulting in a complex spectrum of multimorbidity. The hippocampus-prefrontal cortex (HPC-PFC) circuit emerges as a potential common link between such disorders. However, the mechanisms underlying these outcomes and how they relate to specific behavioral alterations are unclear. We hypothesized that specific dysfunctions of hippocampal-cortical communication due to early-life seizure would be associated with distinct behavioral alterations observed in adulthood. Here, we performed a multilevel study to investigate behavioral, electrophysiological, histopathological, and neurochemical long-term consequences of early-life *Status epilepticus* in male rats. We show that adult animals submitted to early-life seizure (ELS) present working memory impairments and sensorimotor disturbances, such as hyperlocomotion, poor sensorimotor gating, and sensitivity to psychostimulants despite not exhibiting neuronal loss. Surprisingly, cognitive deficits were linked to an aberrant increase in the HPC-PFC long-term

potentiation (LTP) in a U-shaped manner, while sensorimotor alterations were associated with heightened neuroinflammation, as verified by glial fibrillary acidic protein (GFAP) expression, and altered dopamine neurotransmission. Furthermore, ELS rats displayed impaired HPC-PFC theta-gamma coordination and an abnormal brain state during active behavior resembling rapid eye movement (REM) sleep oscillatory dynamics. Our results point to impaired HPC-PFC functional connectivity as a possible pathophysiological mechanism by which ELS can cause cognitive deficits and psychiatric-like manifestations even without neuronal loss, bearing translational implications for understanding the spectrum of multidimensional developmental disorders linked to early-life seizures.

Introduction

The early years of life represent a critical period for neuronal maturation and the development of cognitive functions (Short and Baram, 2019). Disturbances during this period can have a lasting impact on neuronal activity and cause multifaceted neuropsychiatric manifestations (Marín, 2016). Seizures are a prevalent disturbance in the immature brain and are often associated with profound and enduring adverse neurological outcomes that persist throughout adulthood (Brunquell et al., 2002; Holmes, 2009). Children who experience early-life seizures (ELS) not only face an increased likelihood of developing epilepsy but also have a heightened susceptibility to cognitive impairments and behavioral disorders, including autism spectrum disorder (ASD), attention deficit hyperactivity disorder (ADHD), intellectual disability, and psychiatric symptoms like schizophrenia (Dreier et al., 2019; Holmes, 2009; Kaufmann et al., 2009). Since the pathophysiological mechanisms linking ELS and neurodevelopmental disorders are complex, understanding how ELS *per se* affects neuronal function and dissecting the associations between neurobiological and behavioral alterations are crucial for developing better treatments for these conditions.

In experimental models, ELS induces long-term cognitive and behavioral alterations with translational validity with the main neuropsychiatric domains affected in humans (Holmes, 2016). Studies have reported that a prolonged ELS in rodents can lead to cognitive deficits, increased anxiety, reduced social interaction, and facilitated development of epilepsy (Castelhano et al., 2013; De

102 Oliveira et al., 2008a; Kubova et al., 2004). Interestingly, ELS models do not
103 exhibit severe neuronal loss or structural damage (Baram et al., 2002; Sinh et al.,
104 2003), suggesting that the behavioral alterations induced by ELS may be
105 mediated by functional and molecular effects at the brain circuit level
106 (Kandratavicius et al., 2012b, 2012a). The hippocampal-prefrontal cortical circuit
107 (HPC-PFC) plays a crucial role in cognitive and sensorimotor processes, and
108 evidence converges to indicate its dysfunction as a possible common mechanism
109 shared between ELS, neurodevelopmental, and psychiatric disorders, especially
110 epilepsy, psychosis/schizophrenia, ASD, and cognitive disability (Ruggiero et al.,
111 2021; Sigurdsson and Duvarci, 2016). Reports indicate that ELS impacts HPC-
112 PFC functional connectivity, as revealed by the coordination of network
113 oscillations during particular situations (Barry et al., 2020; Kleen et al., 2011;
114 Mouchati et al., 2019; Niedecker et al., 2021). However, how specific functional
115 or molecular effects of ELS on the HPC-PFC network are associated with
116 separate behavioral dimensions within this complex multimorbidity spectrum
117 remains unknown. Also, since behavioral alterations of ELS are long-lasting and
118 progressive, a comprehensive characterization of network dynamics across brain
119 states would be pivotal for a complete understanding of the effects of ELS on
120 brain function.

121 Here, we hypothesized that ELS would produce long-term alterations in
122 HPC-PFC neuronal dynamics related to behavioral abnormalities (Ruggiero et
123 al., 2012). To test this hypothesis, we induced *Status epilepticus* (SE) as a model
124 of prolonged ELS and performed behavioral tests to assess cognitive and
125 sensorimotor processes. Then, we performed neurophysiological,
126 immunohistochemical, and neurochemical experiments to study potential
127 changes in the HPC-PFC circuits that could underlie such behavioral alterations.
128 We found that adult ELS rats present a myriad of behavioral impairments: working
129 memory deficits, hyperlocomotion, poor sensorimotor gating, and behavioral
130 sensitivity to psychostimulants. Surprisingly, we found an enhanced long-term
131 potentiation (LTP) in the HPC-PFC pathway of ELS animals correlated with
132 cognitive impairment in a U-shaped manner. Our results also describe
133 neuroinflammation and alterations in dopaminergic neurotransmission as
134 significant contributors to sensorimotor disturbances. We also investigated HPC-
135 PFC dynamics across different brain states in freely-moving rats. ELS rats

displayed an increased HPC theta power and impaired coordination of PFC gamma activity during active behavior. During rapid eye movement (REM) sleep, ELS rats showed a reduction in HPC-PFC coherence. Remarkably, ELS rats presented an aberrant brain state during active behavior characterized by oscillatory dynamics oddly similar to REM sleep. Finally, we implemented a linear discriminant model, demonstrating that collective patterns of oscillatory alterations accurately distinguished ELS from control animals. Interestingly, although these alterations relate to broad clinical manifestations of neurodevelopmental disturbances and psychiatric manifestations, we recognize a particular convergence of dysfunctional patterns at multiple levels linking the consequences of ELS to functional alterations reported in animal models of epilepsy, psychosis/schizophrenia, ASD, and cognitive disability. These convergent patterns indicate that epileptogenic processes triggered during early life, such as neuroinflammation, could lead to altered neurotransmission and, consequently, aberrant dynamics in the HPC-PFC coordination, potentially contributing to the neurological and psychiatric manifestations linked to early-life seizure.

Materials and Methods

Animals

Wistar rats were housed in a colony room with controlled temperature (22 ± 2 °C) and a 12-h light/dark cycle with free access to food and water. Litters contained up to 8 animals with a maximum of 5 males. Rats were weaned at 21 days postnatally (P21). All procedures were performed according to the National Council for the Control of Animal Experimentation guidelines for animal research and approved by the local Committee on Ethics in the Use of Animals (Ribeirão Preto Medical School, University of São Paulo; protocol: 159/2014).

Experimental Designs

We used four cohorts (a total of 17 litters) to compare the effects of early-life *Status Epilepticus* (ELS) *versus* control (CTRL) animals. The first cohort was used for acute electrophysiology during the induction of ELS (n=5, ELS only). The second was used for behavioral tests (CTRL n=11, and ELS n=14), synaptic

plasticity experiments (CTRL n=7, and ELS n=7), and immunohistochemistry (CTRL n=9, and ELS n=11). The third was used to investigate HPC-PFC dynamics in freely moving rats (CTRL n=6, and ELS n=9). Finally, in the fourth cohort, we assessed behavioral sensitization to psychostimulants (CTRL n=15, and ELS n=14) and neurochemical quantification (CTRL n=8, and ELS n=9).

Early-Life Status Epilepticus

At P11-P12 we induced a 2-hour SE using lithium chloride (LiCl, 127 mg/kg, i.p., Sigma-Aldrich, USA) 18-20 hours prior to injection of methylscopolamine (1 mg/kg, i.p., Sigma-Aldrich) and pilocarpine (80 mg/kg, s.c., Sigma-Aldrich, USA) (Kubová and Mareš, 2013). Behavioral seizures were monitored following the Racine scale (Racine, 1971). SE was interrupted by diazepam (5 mg/kg, i.p., Teuto, Brazil) at the 2-hour mark. During the recovery period (1 week post-ELS) we provided food supplementation and subcutaneous rehydration with saline and monitored body temperature and weight.

Behavior

The radial-arm maze working memory task was based on Floresco et al. (1997). Briefly, rats were kept at 85-90% of their initial body weight throughout the 21 days of the experiment. Training consisted of single daily sessions, each one divided into the training phase and test phase, 30 min apart. During the training session, four doors were kept open providing access to food pellets. In the test session, all doors remained open, but with pellets available only in the four arms that were closed in the previous training session. The sessions were terminated upon full pellet consumption or after 5 min. Two types of errors were quantified: Reference error: reentering arms previously visited during the training session; Working memory error: reentering an arm already visited during the test session. The sum of both categories denoted the total errors for each animal.

Three days after returning to *ad libitum* diet, locomotor activity was evaluated for 30 min in the open field test (Wolf et al., 2016).

Immediately after the open field test, rats were examined for prepulse inhibition (PPI) of the acoustic startle. The PPI test consisted of a habituation period (5 min) followed by 72 trials (intertrial interval: 15 ± 8 s) with prepulse alone (PP), startling pulse alone (P), prepulse followed by a startling pulse (PP + P),

203 and no stimulus, all of which accompanied by background noise (65 dB white
204 noise). Startle-eliciting stimuli were presented at 120 dB for 40 ms (P) and
205 prepulse stimuli were presented for 20 ms (PP, 1000 Hz; 71, 77, and 83 dB; 20
206 ms). Trials were presented in a random order, with each trial type being presented
207 six times. We used the equation: %PPI = 100 − 100 × (mean startle amplitude at
208 PP + P)/(mean startle amplitude at P) (Wolf et al., 2016).
209 In order to measure the effects of ELS on sensitization to
210 psychostimulants, we performed the apomorphine-induced locomotion test. At
211 P80-90, rats were placed in the open field apparatus and were allowed to roam
212 for 60 min. Then, we injected apomorphine (APO, 1.5 mg/kg, i.p., Sigma-Aldrich,
213 USA) and measured locomotion for another 60 min. The distance across blocks
214 was normalized by Z-score to the mean of baseline blocks.
215
216 ***Synaptic Plasticity***
217 HPC-PFC synaptic plasticity studies were performed as described in
218 previous works from our group (Bueno-Junior et al., 2018; Ruggiero et al., 2018).
219 Briefly, rats were anesthetized with urethane (1.2 mg/Kg in NaCl 0.15 M, i.p.) for
220 electrode implantation. A recording electrode (Teflon-coated tungsten wires 60
221 µm, AM-Systems) was inserted in the medial PFC (prelimbic region (PL),
222 anterior-posterior: 3.0 mm; medial-lateral, ML: 0.5 mm; dorsal-ventral, DV: 3.2
223 mm), and a bipolar stimulation electrode (twisted wires; ~500 µm inter-pole
224 distance) was inserted in the ipsilateral HPC (intermediate CA1 AP: −5.6 mm;
225 ML: 4.5 mm; DV: 2.5 mm). An additional burr hole was drilled over the right
226 parietal cortex for a reference screw. Temperature was kept constant at 37 ±
227 0.5°C during the experiment.
228 HPC was stimulated with single monophasic pulses (200 µs, 0.05 Hz,
229 150–300 µA, 80-ms inter-pulse interval) while recording PFC field postsynaptic
230 potentials (fPSPs). Stimulation intensity (60–500 µA) was calibrated to evoke 50–
231 60% of the maximal fPSP amplitude. Field recordings were conditioned through
232 a preamplifier (100× gain, 0.03–3 kHz bandpass; Grass) and digitized at 10 kHz
233 (ADInstruments). For LTP induction, we used a high-frequency stimulation (HFS)
234 protocol consisting of 2 series (10 min apart) of 10 trains (0.1 Hz), each train with
235 50 pulses at 250 Hz (Ruggiero et al., 2018). fPSP amplitudes and slopes were
236 computed as the difference and slope between the positive and negative peaks,

237 respectively. Short-term synaptic plasticity was estimated by paired-pulse
238 facilitation (PPF), calculated as the ratio of the fPSP2 and fPSP1 (Lopes-Aguiar
239 et al., 2020). Amplitudes and slopes were normalized as ratios of the baseline
240 mean and averaged into 10-min bins.
241
242 ***Brain Tissue Processing***
243 *Immunohistochemistry*
244 We employed a standardized immunohistochemistry protocol (Peixoto-
245 Santos et al., 2015) to estimate NeuN+ neuronal density and to evaluate
246 parvalbumin-expressing (PV) interneurons, mGluR5 expression, and glial
247 fibrillary acid protein (GFAP) reaction. Briefly, endogenous peroxidases were
248 blocked and the antigens were exposed by microwave-induced retrieval. We
249 used the primary antibodies against NeuN (Chemicon, USA; 1:1000), PV
250 (Calbiochem, USA; 1:500), mGluR5 (Millipore, USA; 1:200), and GFAP (Dako,
251 Denmark; 1:500) proteins, and biotinylated secondary antibodies (Dako,
252 Denmark; 1:200). Revelation was performed with Elite ABC Kit (Vector) and
253 diaminobenzidine solution (Pierce).
254 Images from the regions of interest were captured at 200× magnification
255 in the Axio Scope.A1 microscope system (Carl Zeiss). The regions of interest
256 included the hippocampus (CA1 and GL, granule layer of dentate gyrus),
257 entorhinal cortex (EC), infralimbic (IL) and prelimbic cortex (PL), and thalamic
258 reticular nucleus (TRN). Images were then processed in Image J software (NIH,
259 USA; 1.48v). Data are shown as the density of NeuN positive cells and
260 immunopositive area for PV, mGluR5, and GFAP.
261
262 *High-Performance Liquid Chromatography (HPLC)*
263 Samples were taken bilaterally from the nucleus accumbens (NAc), PFC,
264 and HPC. The samples were homogenized with ultrasound in a 0.1 mol/L $HClO_4$
265 0.02% $Na_2S_2O_2$ solution containing dihydroxybenzylamine (DHBA, 146.5 ng/mL),
266 and homoserine (HSER, 10 µg/mL) as internal standards and at a dilution of 15
267 µL per sample milligram. We employed Shimadzu LC-10AD isocratic systems
268 with a fluorescence detector for glutamate (Glu) and gamma-aminobutyric acid
269 (GABA), and an electrochemical detector for dopamine (DA) and its metabolites
270 3,4-dihydroxyphenylacetic acid (DOPAC) as previously published (Castro-Neto

et al., 2013). The neurotransmitter levels were considered to reflect neurotransmitter stock in synaptic vesicles, their metabolites reflected the release, and metabolite/neurotransmitter ratios were taken as an index of neurotransmitter turnover. Standards containing all amino acids and monoamines/metabolites of interest were employed to define their respective peaks in the samples.

Freely Moving Electrophysiology

Electrophysiological recordings

Chronic head caps consisted of two eight-channel connectors (Omnetics), one for the PFC (PL, 7 wires) and another for the HPC (intermediate CA1, 7 wires) (Bueno-Junior et al., 2017; Marques et al., 2022). We additionally implanted a recording wire into the trapezius muscle to serve as an electromyogram (EMG). The EMG wire was soldered to the HPC connector. Microscrews were fastened into the skull, including a ground reference in the intraparietal area. Animals were allowed to recover for 8-9 days before recordings.

To record electrophysiological signals through sleep-wake states, rats were placed into a shuttle box apparatus inside a soundproof box with food and water *ad libitum*. Recordings varied between 30 to 48 hours, divided later into periods of 6 hours for analysis. Local field potentials (LFP) were recorded through a multichannel acquisition processor (Plexon) (1000× gain, 0.7-500 Hz bandpass filter, 1-kHz sampling rate).

Classification of sleep-wake states

Classification of the sleep-wake cycle states was carried out through a semi-supervised machine learning pipeline. The HPC theta (4.5-12 Hz), PFC delta (0.7-4 Hz), and EMG (100-200 Hz) power were computed in 5-second epochs without overlaps (4 tapers; time-bandwidth product: 2.5). A support vector machine (SVM) (radial basis function) was trained to discriminate the epochs into: (1) awake or sleep epochs using EMG power; (2) REM or NREM epochs based on theta/delta ratio; (3) quiet wake (QWK) or active (ACT) epochs based on theta/delta ratio. Later, we classified our recordings based on 30-second epochs by grouping sets of six 5-second epochs and considering the most representative state.

Spike wave-discharge detection (SWD)

For spike wave-discharge detection, we used the PFC recordings. First, the short-time Fourier transform (STFT) was computed within 3-70 Hz throughout 250-ms windows with 50% overlap. A detection threshold was defined as the mean + 1.5 standard deviation of the absolute value of the STFT of the frequency bands 4.4-16.4, 17.6-32.8, and 35.1-55 Hz throughout the entire recording. SWD events were detected when the average STFT of the aforementioned frequency bands at one epoch exceeded the threshold. Consecutive epochs above the threshold were grouped as the same event. The beginning and the end of an event were defined as the closest epochs when the average STFT was lower than the mean + 1 standard deviation of STFT of the frequency bands of interest. Lastly, the detected putative events were manually sorted by an expert.

Spectral estimates

We divided 30-s epochs into 3-s epochs for spectral analyses. Power spectrum densities (PSD) and magnitude-squared coherence were obtained using Welch's method with 1-s segments, 50% overlap, and Hamming windowing. Relative power was obtained by dividing values by the sum within 0.5-55 Hz for each epoch. We defined the frequency bands: delta (1-4 Hz), theta (4.5-11 Hz), low gamma (30-55 Hz), and high-gamma (65-100 Hz) to compare estimates and obtained the spectral peak of each epoch using MATLAB function *findpeaks*.

To quantify theta oscillation power we used the FOOOF algorithm (Donoghue et al., 2020), which parametrizes the PSD separating the periodic and aperiodic components of the signal. We used frequencies within 3-40 Hz, the “fixed” aperiodic mode, a minimum peak height of 0.05, and a maximum number of peaks of 4 (https://fooof-tools.github.io/fooof/). EMG data were low-cut filtered (>30 Hz) and the sum of power within 30-200 Hz was obtained.

As a synchrony measure, we also computed cross-correlations between each pair of LFPs (low-pass filter of 50 Hz) recorded from the HPC and PFC using a maximum lag of 1 s. Coefficients were normalized so that the autocorrelations at zero lag were one. We observed that the highest coefficients occurred in the range of -80 to -20 ms (HPC leading the PFC), so we obtained the maximum

339 coefficient within this range for each rat average for comparisons. Cross-
340 spectrum power was calculated using Welch's method for the normalized
341 correlation coefficients from -1 to 1 s.
342 For cross-frequency amplitude spectrum correlations, we computed the
343 absolute STFT for each 3-s epoch throughout 100-ms segments with 50%
344 overlap and Hamming windowing across 0.5-Hz frequency bins within 0.5-200
345 Hz. We calculated the correlation matrix for each frequency pair using Pearson's
346 R.
347
348 *State maps*
349 After state classification and spectral analysis, we computed two-
350 dimensional state maps to investigate the natural distinction between sleep-wake
351 states. The state maps were computed according to Gervasoni et al. (2004) and
352 Dzirasa et al. (2006). First, we obtained the power *ratio 1* (4.5-9/4.5-50 Hz) and
353 *ratio 2* (2-20/2-50 Hz) for each region and the first principal component, estimated
354 by singular value decomposition algorithm considering both regions, for each
355 ratio. Finally, we applied a Hann window of 10 epochs on scores throughout time
356 for smoothing.
357 To identify the intermediate states (IS), we first estimated the trajectory
358 *speed* of epochs throughout state map dimensions as the Euclidean distance
359 between each epoch and its predecessor. Then, we defined a threshold of 0.1
360 and labeled the epochs with greater speed as IS. This threshold was determined
361 heuristically, corresponding closely to the expected value plus a standard
362 deviation from a Poisson distribution across rats.
363 From visual inspection and the literature (Dzirasa et al., 2006; Gervasoni
364 et al., 2004), the state maps usually separate three well-defined clusters
365 heuristically corresponding to awake, REM, and NREM sleep. To assure the
366 correspondence between state map clusters and the classification outcomes, we
367 performed Gaussian mixture models clustering of the state maps for 3 clusters
368 and 80% posterior probabilities and computed Chi-squared tests with the
369 classified NREM, REM, and awake (QWK+ACT) labels. Three animals were
370 excluded for having outlier lower Chi-values. Although QWK and ACT states are
371 often evenly distributed inside the awake cluster, QWK epochs may overlap with
372 intermediate states closer to NREM, so the ACT epochs were considered to

represent more precisely the localization of neural dynamics associated with behavior in the state map. The dissimilarity between ACT and REM states was estimated by the average pairwise state map Euclidean distance of all epochs between the two states.

We used machine learning algorithms to decode sleep-wake states from the state map. We used the ACT and REM state map *ratios 1* and *2* values. We applied a linear and radial basis function SVM *fictcsvm* function in MATLAB ('KernelFunction', 'linear' or 'rbf') as well as a Random Forest algorithm using the *fitcensemble* function in MATLAB ('Method', 'bag', 'NumLearningCycles', 50, for Random Forest) to decode states. We used the ACT and REM epochs from all the rats creating one single model for the CTRL or ELS condition. Using the same approach, we also constructed a random forest decoder model with non-reduced variables using 1 to 55 Hz (0.5 Hz bins) for the PFC and HPC power and coherence. Discrimination was evaluated using the area under the receiver operating characteristic curve (AUC-ROC). The point-wise confidence interval was calculated using a 1000-repetition bootstrap. Average AUC-ROC values were calculated using the prediction of the trained model on 20% of the epochs as test data and repeating the process 100 times.

Statistical Analysis

Data were analyzed using GraphPad Prism Software version 9.00 (GraphPad Software, LLC), and R studio version 2021. We used paired Student *t*-tests for within-group comparisons and two-sample *t*-tests for between-group comparisons. Two-way ANOVA with repeated measures (RM) was performed for comparisons across time bins, using Sidak's multiple comparison test as a *post-hoc*. To examine linear model assumptions, we analyzed the distribution of the residuals using a Q-Q plot, the Kolmogorov-Smirnov test, homoscedasticity, and the residual plot. We used the Mann-Whitney test to compare two groups and the Wilcoxon signed-rank test to paired comparisons as non-parametric alternatives. We calculated Pearson's linear correlation and Spearman's rank correlation as a nonparametric equivalent. To compare correlation and spectral coherence estimates we applied Fisher's Z transform to the data. For multiple comparisons in the neurochemical quantification, we performed Holm's procedure for multiple comparisons correction across neurotransmitters and metabolites per region.

Data are expressed as the mean ± SEM. The significance level was set to 0.05 unless stated otherwise. For some multiple comparisons, statistical values are expressed as the range. Significances are expressed as $^{\dagger}p < 0.1$, $^{*}p < 0.05$, $^{**}p < 0.01$, and $^{***}p < 0.001$.

Linear mixed-effects models

We also constructed statistical inferential models across time controlling for individual variability and litter using linear mixed-effects models. We compared power and coherence estimates throughout time by dividing the electrophysiological recording into 5 periods (6 hours). Group and time (periods) were assigned as fixed effects and subject, litter, and time were assigned as random effects. We used this approach to construct a maximal random effects structure model as preconized in the literature as more generalizable (Barr et al., 2013). The model was estimated by restricted maximum likelihood using the *lme* function of the *nlme* package (Pinheiro et al., 2023) with an unstructured covariance matrix.

Multivariate analysis

Each variable was Z-scored before multivariate analysis. We constructed correlograms to assess the relationship within behavioral and neurobiological measures. Variables were sorted by agglomerative hierarchical clustering using Ward's method and correlation as the metric. We also performed agglomerative hierarchical clustering of subjects using Ward's method and Euclidean distance as the metric to assess how unsupervised clustering by our multivariate data might match the experimental groups. An optimal number of clusters was estimated using the silhouette method and final definition was based on parsimonious interpretability of the results.

Principal component analysis (PCA), using singular-value decomposition, was used for dimensionality reduction to find collective patterns of variance within behavioral variables (behavior factors) and neurobiological variables (neurobiology factors), and to reduce each immunohistochemical measure across all brain regions into single scores. Principal components (PCs) were projected onto data and the mean score was compared between conditions.

440 Canonical correlation analysis (CCA) was performed to describe
441 multivariate relationships between behavioral and neurobiological measures.
442 Missing data were imputed using the multiple imputation by chained equations
443 algorithm. For CCA, we used the first PC (PC1) and second PC (PC2) of
444 behavioral variables as inputs for the behavioral factors and the PC1 of each
445 immunohistochemical variable (NeuN, PV, mGluR5, and GFAP,) across all brain
446 regions and the Z-scored LTP data as inputs for the neurobiological factors.
447 Variables were narrowed down from 30 to 7, which is statistically appropriate for
448 our sample size. We used the CCA package in R to obtain the canonical
449 dimensions and performed the Hotelling-Lawley trace statistic to assess the
450 significance of each dimension.
451 We used multivariate generalized linear models (GLM) with a Gaussian
452 family and an identity link function. Quasi-Poisson regression (quasi-Poisson
453 family and logarithmic link function) were used for count data with overdispersion
454 (Errors in the radial maze) using a quadratic covariate (LTP). We constructed two
455 types of models: 1) a full model considering all the covariates; and 2) a restricted
456 model using backward stepwise model selection based on the Akaike information
457 criterion.
458 To assess the effectiveness of neurophysiological features in
459 discriminating CTRL from ELS rats, we fitted a regularized linear discriminant
460 classifier model on the PCA scores of selected electrophysiological variables. We
461 used the MATLAB function *fitcdiscr* without hyperparameter optimization. The
462 linear classifier using two predictors allowed the graphical representation and
463 avoided the overfitting of a high number of variables. Accuracy was determined
464 as the probability of correct category assignments using leave-one-out cross-
465 validation. We also determined the contribution of each original
466 neurophysiological variable by assessing their respective AUCs using a
467 univariate logistic regression model.
468
469 **Results**
470 **ELS induces cognitive and behavioral impairments in adulthood**
471 SE induced by lithium-pilocarpine in early life (Fig. 1A) produced an
472 unequivocal and stereotyped seizure, consisting mainly of forelimb myoclonus
473 and orofacial automatism (Racine 3), with some animals showing further

474 development into bilateral forelimb myoclonus, rearing and falling (Racine 4 and
475 5) (Racine, 1971). Seizures were confirmed electrophysiologically in freely
476 moving recordings of the frontal cortex and HPC, with paroxysms starting 10 min
477 after pilocarpine injection and persisting for at least 120 min (Fig. 1B).

478 Next, we investigated the long-term behavioral consequences of ELS (Fig.
479 2A). First, we evaluated possible weight differences as a confounder of
480 behavioral measures. ELS rats displayed weight loss on the day after SE (Two-
481 way RM ANOVA, treatment effect: $F_{(9,207)} = 11.7$, $p < 0.0001$, Sidak's *post-*
482 *hoc:* $p < 0.0001$; Fig. 2B). However, ELS animals recovered the pace of normal
483 weight gain in the subsequent days (*post-hoc*: $p > 0.05$) and into adulthood (Fig.
484 2C), showing no distinction to CTRL before (*t*-test, $t_{(23)} = 1.440$, $p = 0.1634$) or
485 during food restriction (*t*-test, $t_{(23)} = 0.0535$, $p = 0.9577$), indicating that behavioral
486 effects were unrelated to weight differences or alterations in food-seeking.

487 Importantly, when examined for spatial memory in the radial-arm maze,
488 ELS rats presented a specific increase in working memory errors (Mann-Whitney
489 test, $U = 36.5$, *n(CTRL, ELS)* = 11, 14, $p = 0.0254$; Fig. 2D). We found no
490 differences in the total reference errors (*t*-test, $t_{(23)} = 1.719$, $p = 0.0991$; Fig 2D)
491 and in the learning curve (Two-way RM ANOVA, treatment effect: $F_{(1,23)} =$
492 0.8032, $p = 0.3794$; Fig 2E). In addition, ELS rats exhibited significantly higher
493 locomotion in the open field test (Mann-Whitney test, $U = 27$, *n(CTRL, ELS)* =
494 11/14, $p = 0.0051$; Fig. 2F). ELS rats also displayed a higher startle response (*t-*
495 test, $t_{(23)} = 2.757$, $p = 0.011$; Fig. 2G) and a deficit in sensorimotor gating
496 represented by a reduction in PPI of the acoustic startle (Two-way RM ANOVA,
497 treatment effect: $F_{(2,46)} = 19.6$, $p < 0.0001$, Sidak's *post-hoc:* PPI 71 dB: $p =$
498 0.0017; PPI 77 dB: $p = 0.1040$; PPI 83 dB: $p = 0.030$; Fig. 2H).

499 Interestingly, all these behavioral alterations are described in animal
500 models of neurodevelopmental disorders such as ASD and schizophrenia (Ey et
501 al., 2011; Scott et al., 2018; Sigurdsson, 2016). We investigated if collective
502 patterns of behavioral alterations induced by ELS could reflect latent factors
503 representing more comprehensive behavioral dimensions. Working memory
504 errors in the radial-arm maze showed little correlation with the other behavioral
505 variables, while sensorimotor variables (locomotion, startle response and
506 sensorimotor gating) presented a strong correlation with each other. PPI
507 exhibited a positive correlation with every intensity and a negative correlation with

508 startle response and locomotion (Fig. 2I). We also performed PCA to extract
509 patterns of variance between multivariate behavioral data (Fig. 2J-M). Our
510 analysis indicated that dimensionality reduction by PCA using the first two
511 components explained 71.32% of the variability of the data (Fig. 2J). By analyzing
512 the loadings of the PC1, the variables that contribute more strongly (>0.5) to this
513 dimension were: high total distance, startle reflex, and low PPI scores, indicating
514 this component represents a latent factor of sensorimotor dysfunction. In turn, the
515 PC2 represents the cognitive dimension of the behavioral variables, as it presents
516 a high loading value (>0.5) for working memory errors (Fig. 2K). Finally, we found
517 that these PCs clearly distinguished CTRL from ELS animals, which presented
518 higher values of PC1 (PC1: *t*-test, $t_{(23)} = 3.9713$, $p = 0.0006$; PC2: *t*-test, $t_{(23)} =$
519 1.6466, $p = 0.1132$; Fig. 2L-M). These results indicate that the covariance across
520 behavioral tests can be summarized by a latent *sensorimotor factor* (PC1) and a
521 *cognitive factor* (PC2), representing two distinct dimensions of the behavioral
522 phenotype and suggesting possibly different neurobiological bases.
523
524 **Aberrant HPC-PFC synaptic plasticity in animals submitted to ELS**
525 Next, we tested the hypothesis that behavioral abnormalities in ELS rats
526 could be associated with synaptic plasticity impairments of the HPC-PFC
527 pathway (Fig. 3A-C). First, we looked for ELS-related alterations in basal synaptic
528 efficacy before inducing LTP. Synaptic efficacy was assessed in terms of basal
529 fPSP amplitude and slope (amplitude: *t*-test, $t_{(12)} = 1.278$, $p = 0.2255$; slope: *t*-
530 test, $t_{(12)} = 0.5470$, $p = 0.5944$; Fig. 3D), input-output curve (fPSP amplitude as a
531 function of stimulus intensity) (Two-way RM ANOVA, treatment effect: $F_{(1,12)} =$
532 0.6596, $p = 0.4325$; Fig. 3E) and PPF curve (PPF as a function of the inter-pulse
533 interval) (Two-way RM ANOVA, treatment effect: $F_{(1,12)} = 0.3345$, $p = 0.5737$;
534 Fig. 3F). None of these measures indicated alterations in ELS when compared to
535 CTRL (Fig. 3D-F).
536 Then, we proceeded to the synaptic plasticity experiments and found that
537 ELS rats presented an abnormally augmented LTP compared to CTRL (Fig. 3G;
538 Two-way RM ANOVA, treatment effect: $F_{(1,12)} = 7.54$, $p = 0.0177$; interaction
539 effect: $F_{(26,312)} = 7.393$, $p < 0.0001$; Sidak's *post-hoc:* $p < 0.05$ for 10-60 min; *t*-
540 test, $t_{(12)} = 2.747$, $p = 0.0177$; Fig. 3G inset), despite the lack of alterations in
541 basal synaptic efficacy described above (Fig. 3D-F). Aberrant LTP in the ELS rats

542 was also observed when analyzing the fPSP slope (Two-way RM ANOVA,
543 treatment effect: $F_{(1,12)}$ = 4.757, p = 0.0498; interaction effect: $F_{(26,312)}$ =
544 4.120, $p < 0.0001$; Sidak's *post-hoc:* $p < 0.05$ for 10-40 min; Fig. 3H; *t*-test, $t_{(23)}$ =
545 2.794, p = 0.0162; Fig. 3H inset). However, short-term plasticity measured by
546 PPF decreased during the initial 30 min of recording (Two-way RM ANOVA,
547 interaction effect: $F_{(26,312)}$ = 3.457, $p < 0.0001$; Sidak's *post-hoc:* $p < 0.05$ for 20-
548 30 min; Fig. 3I), possibly reflecting a ceiling effect on fPSP amplitude after LTP
549 induction. With these results, we demonstrate that, although ELS does not affect
550 basal synaptic efficiency, it significantly increases the ability of HPC-PFC circuits
551 to undergo LTP.
552
553 **ELS induces long-term neural inflammation, but not neuronal loss**
554 We sought to investigate histopathological alterations in cortico-limbic
555 circuits that could underlie the abnormalities in behavior and HPC-PFC synaptic
556 plasticity of ELS rats (Fig. 4A). In accordance with previous findings, ELS rats did
557 not present neuronal loss when adults (Mixed-effects model, $F_{(1,12)}$ = 0.7683, p =
558 0.3980; uncorrected Mann-Whitney test, p = 0.1666-0.9372; Fig. 4B). Also, ELS
559 did not produce long-term effects in the expression of PV (Mixed-effects
560 model, $F_{(1,13)}$ = 0.008, p = 0.9297; uncorrected Mann-Whitney test, p = 0.3659-
561 0.9307; Fig. 4C) or mGluR5 receptors (Mixed-effects model, $F_{(1,11)}$ = 0.0011, p =
562 0.9735; uncorrected Mann-Whitney test, p = 0.2467-0.8181; Fig. 4D). Finally, we
563 found a strong increase in neuroinflammation, verified by the marked expression
564 of GFAP in ELS rats in all regions investigated except the infralimbic cortex
565 (Mixed-effects model, $F_{(1,18)}$ = 5.368, p = 0.0325; uncorrected Mann-Whitney test,
566 p = 0.0067-0.0419 for GL, CA1, EC, PL, and TRN, and p = 0.2298 for IL; Fig. 4E).
567 These results show that ELS produces subsequent brain inflammation. Also,
568 important cognitive and behavioral impairments can manifest even in the
569 absence of substantial neuronal loss in the HPC or PFC.
570
571 **Cognitive impairment and sensorimotor disturbances are distinctly**
572 **correlated with abnormal LTP and neuroinflammation**
573 By understanding the association between behavioral and neurobiological
574 variables, we would be able to infer putative mechanisms underlying the
575 behavioral comorbidities observed in ELS animals. To investigate multivariate

576 relationships between the behavioral (cognitive and sensorimotor factors) and
577 neurobiological (synaptic plasticity and immunohistochemical measures)
578 dimensions of ELS effects, we conducted CCA (Fig. 5A). CCA produced a
579 significant high-correlation model ($r = 0.94$, Hotteling-Lawley trace test, *F-*
580 *approximation*$_{(10,12)} = 3.2311$, $p = 0.0164$; Fig. 5B) that clearly separated CTRL
581 from ELS (behavior canonical dimension, *t*-test, $t_{(11)} = 3.693$, $p = 0.0035$;
582 neurobiology canonical dimension, *t*-test, $t_{(11)} = 3.917$, $p = 0.0024$; Fig. 5C). By
583 analyzing the coefficients, we observed that the behavior canonical dimension
584 showed higher values for the sensorimotor factor, but also included the cognitive
585 factor, although at a lower degree (Fig. 5D). The neurobiology canonical
586 dimension showed a larger value for the GFAP, intermediate values for LTP and
587 PV and the lowest coefficients for NeuN and mGluR5 (Fig. 5D). A similar pattern
588 was observed when analyzing the loadings for each dimension (Fig 5E). Notably,
589 the neurobiological variables have only weak correlations between them (Fig.
590 5F). To further dissect specific multivariate relationships between behavioral and
591 neurobiological measures, we constructed generalized linear models (GLM). The
592 GLM indicates GFAP, PV, and LTP as the most significant variables that explain
593 the sensorimotor factor variance (coefficients = 2.3775, 0.8457, and 0.5187; p =
594 0.1164, 0.00548, 0.08474 for GFAP, PV, and LTP, respectively, (Fig. 5G).
595 Accordingly, GLM multivariate regression indicates a strong association between
596 the sensorimotor factor and all significant GLM coefficients (GFAP, PV, plus LTP:
597 $r^2 = 0.7974$, $p = 0.0116$; Fig. 5H), as well as sensorimotor factor and univariate
598 neurobiological measures (GFAP: $r = 0.6840$, $p = 0.0099$; Fig. 5I, PV: $r = 0.6548$,
599 $p = 0.0151$; Fig. 5J). Strikingly, we found a quadratic relationship between
600 synaptic plasticity effects and measures of cognitive impairment. Poor
601 performance on the working memory test was observed in rats that presented too
602 low or too high values of HPC-PFC LTP, suggesting a U-shaped relationship
603 between LTP and cognitive performance (Fig. 5K-L). We observed this quadratic
604 relationship using both the cognitive factor (gaussian GLM, LTP coefficient =
605 1.22, $p = 0.0162$; Fig. 5K) and raw error values from the radial maze test using a
606 quasi-Poisson GLM ($p = 0.00843$; Fig. 5L).

607 Taken together, both neuroinflammation and synaptic plasticity alterations
608 may underlie the behavioral effects of ELS, with neuroinflammation being more

associated with the sensorimotor dimension and LTP with the cognitive dimension.

ELS animals present epileptiform-like activity when adults

Given the results above, we decided to further investigate the relationships between circuit dynamics and behavioral dysfunctions during different brain states using chronic electrophysiology recordings. We classified LFP epochs into active wake (ACT), non-REM (NREM) sleep, rapid eye movement sleep (REM), and quiet wake (QWK; Fig. 6A-D). No CTRL *vs.* ELS differences were found in sleep architecture, according to the mean consecutive duration of each state, percentage of time awake, number of persistent episodes in each state (Two-way RM ANOVA, $F_{(1,13)} = 0.6500$, $p > 0.4346$; Fig. 6E-G), and percentage of time in each state (Two-way RM ANOVA, $F_{(1,13)} = 0.5425$, $p > 0.4745$; Fig. 6H).

We also examined if ELS animals presented ictal activity during recordings. We found that 44.45% of the ELS animals presented electrographic discharges similar to spike-wave discharges (SWD) or rhythmical spiking (Fig. 6H-I). SWDs occurred mainly during NREM sleep and less often in QWK and ACT but rarely occurred during REM epochs (Fig 6J-M). The SWDs were not found in the CTRL rats, indicating that ELS induces an epileptogenic process.

Increased HPC theta power during behavioral activity in ELS animals

We initially concentrated our investigation on the ACT behavioral state to associate oscillatory patterns with the behavioral abnormalities observed. We found that ELS animals presented a higher theta power during ACT states in the HPC (*t*-test, $t_{(13)} = 2.259$, $p = 0.0417$; Fig. 7A-D), but not in the PFC (*t*-test, $t_{(13)} = 0.2636$, $p = 0.7961$; Fig. 7B). This increased theta activity is more prominent during the first periods of recording and exploration of the new environment (linear mixed-effects model, $t = 2.10$, $p = 0.055$; Uncorrected *t*-tests for period comparison: $t_{(13)} = 2.145$, 2.367, and 2.319, $p = 0.051$, 0.034, and 0.037 for periods 1, 2, and 3, respectively; Fig. 7E). To further explore whether theta power increase reflects a true oscillation and is not due to alterations in the aperiodic components of the PSD, we also performed a PSD parametrization to separate the theta oscillation (Fig. 7F). We found an increase in the theta oscillatory activity in ELS animals during ACT states, indicating an actual oscillatory effect (Mann-

643 Whitney, U = 7, n = (6,9), p = 0.0176; Fig. 7G-H). Hippocampal theta is well
644 known to occur during periods of locomotor activity, e.g., postural changes, head
645 movements, and rearing (Buzsáki and Moser, 2013) representing a possible
646 confounder. To control for this, we co-examined HPC theta power and EMG
647 distributions during active states in CTRL *vs.* ELS rats (Fig. 7I). Indeed, theta
648 oscillatory increase in ELS animals did not appear to be related to more
649 movement, as we did not observe a significant association between EMG and
650 theta power. In contrast, we found higher theta power in ELS animals even at low
651 levels of EMG activity (Fig. 7I).
652
653 **ELS promotes abnormal gamma coordination in the PFC during behavioral**
654 **activity**
655 Considering the extensively documented involvement of PFC gamma
656 activity in cognitive and sensory processes, as well as its alterations observed in
657 animal models of neurodevelopmental and psychiatric disorders such as ASD
658 and schizophrenia (Rojas and Wilson, 2014; Sigurdsson, 2016), we investigated
659 the possible effects of ELS on PFC gamma activity during active states. ELS
660 animals showed a reduced theta-gamma amplitude correlation during ACT states
661 (t-test, $t_{(13)}$ = 2.851, p = 0.0136; Fig. 8A-C), indicating that high-gamma activity is
662 less coordinated, despite the increase in theta power. Interestingly, there were
663 no increases in both low or high-gamma power (low-gamma: Mann-Whitney, U =
664 16, n = (6,9), p = 0.2238; high-gamma: Mann-Whitney, U = 24, n = (6,9), p =
665 0.7756; Fig. 8D). Amplitude correlation is an indicator of large-scale cortical
666 interactions that govern cognition (Siegel et al., 2012). Thus, the lower theta-high
667 gamma correlations found here may be related to the cognitive disruptions
668 caused by ELS.
669 Next, we found a reduction in the PFC spectral exponent in ELS animals
670 assessed by aperiodic PFC activity during ACT state (note the flatter spectra of
671 ELS in Fig. 8E), distribution of the aperiodic component (exponent and offset, Fig
672 8F), and comparison in exponent parameter between groups (t-test, $t_{(13)}$ =
673 2.010, p = 0.0656; Fig. 8G). Reductions of the spectral exponent have been
674 discussed to indicate increased excitation/inhibition imbalance (Gao et al., 2017).
675 This abnormal gamma dynamics in the ELS indicates a less coordinated

oscillatory activity, which may reflect impaired limbic-cortical or cortico-cortical interactions that underlie cognitive dysfunctions.

ELS impairs HPC-PFC coherence during REM sleep

HPC-PFC connectivity and information flow during REM sleep is essential for memory consolidation (Lesting et al., 2013). Because we found cognitive impairments in ELS animals, we investigated HPC-PFC interactions during REM. First, we observed that the theta power in the PFC and HPC during REM is not different between groups (PFC: *t*-test, $t_{(13)} = 1.320$, $p = 0.2096$; HPC: *t*-test, $t_{(13)} = 0.3557$, $p = 0.7278$; Fig. 9A-B). However, we found that ELS rats show reduced HPC-PFC connectivity in the theta band, measured by spectral coherence during REM sleep (*t*-test, $t_{(13)} = 2.183$, $p = 0.0480$; Fig. 9C-D). This difference is present throughout the entire recording, as observed by the comparisons for all 6-hour periods (linear mixed-effects model, $t = -2.27$, $p = 0.0408$; Fig. 9D, right). We further confirmed this difference by analyzing the cross-correlation and cross-spectrum power of the HPC-PFC LFP during REM (Fig. 9E-G). Cross-correlation analysis reveals a clear directionality between signals from the HPC to the PFC in both groups that happens markedly at a specific lag (-80 to -20 ms; Fig. 9E), in which ELS rats present the most profound decrease in the correlation peak (*t*-test, $t_{(13)} = 2.533$, $p = 0.0250$; Fig. 9F-G).

We noticed from inspecting the theta coherence changes between ACT and REM – the two states with the strongest theta coherence – that all CTRL animals exhibited greater theta coherence during REM (paired *t*-test, $t_{(5)} = 8.023$, $p = 0.0005$; Fig. 9H), while in the ELS group, part of the animals did not present such an increase (paired *t*-test, $t_{(8)} = 1.924$, $p = 0.09$; Fig. 9H). This dynamic is further illustrated by observing the coherence changes across REM, QWK, and ACT states. While most CTRL rats present an inclined decrease from REM to QWK and a slight increase from QWK to ACT, ELS rats display a flatter curve (Fig. 9I). By quantifying the homogeneity of the distributions of average theta coherence values across states with entropy, we found a significantly higher entropy (more homogeneous) in ELS than CTRL (paired *t*-test, $t_{(13)} = 2.695$, $p = 0.0184$; Fig. 9J). These results indicate that ELS promotes impairment in HPC-PFC connectivity during REM sleep and in the regulation of state-dependent dynamics.

710

711 **ELS rats display REM-like oscillatory dynamics during active behavior**

712 After we noticed that ELS animals show less distinction of some
713 electrophysiological activities between states, particularly REM and ACT, we
714 decided to further characterize the long-term effects of ELS on HPC-PFC state-
715 dependent oscillatory dynamics across the sleep-wake cycle. For that, we
716 constructed a state map based on two spectral power ratios (Dzirasa et al., 2006;
717 Gervasoni et al., 2004). This state map framework allows consistent
718 characterization of all major brain states, revealing a dynamic global structure
719 produced by the collective activity of forebrain structures (Gervasoni et al., 2004).
720 First, we verified that the state maps reflected other brain and muscle activities
721 that were not directly used for the map construction, such as the concentrated
722 distribution of the PFC delta power during NREM, of the HPC theta/delta ratios in
723 REM, of the EMG power in awake states, and of HPC-PFC theta coherence in
724 both REM and awake states (Fig. 10A). Thus, as expected, our state maps
725 presented three distinct clusters that precisely located REM, NREM, and ACT
726 epochs (Fig. 10B).

727 Using this approach, a previous study reported an overlap between awake
728 and REM states in a hyperdopaminergic mouse model (Dzirasa et al., 2006).
729 Because we found ELS-related functional changes specifically during ACT and
730 REM, we sought to investigate the convergence between these two states.
731 Remarkably, we also found that ELS rats showed a significant similarity between
732 the REM and ACT states (Fig. 10B). While in CTRL rats the distributions of
733 Euclidean distances were larger, homogeneous, and symmetrical (Fig. 10C),
734 ELS rats presented highly variable patterns across animals, most of which with
735 skewed distributions concentrated at shorter distances (Fig. 10C). Indeed, the
736 Euclidean distance was significantly reduced in ELS (*t*-test, $t_{(13)} = 2.326$, $p =$
737 0.0369; Fig. 10D), suggesting that the spectral features of REM and ACT are
738 more similar in ELS animals.

739 Interestingly, we observed that this difference in states similarity was
740 stronger in the initial 12 hours of recording, which corresponds to the periods of
741 habituation to the novel environment (*t*-test, for periods 1-2: $t_{(13)} = 2.45$, $p = 0.029$;
742 for periods 3-4: $t_{(13)} = 0.9409$, $p = 0.3638$; Fig. 10E).

743 To further demonstrate the higher similarity between REM and ACT states
744 in ELS animals, we used machine learning algorithms in an attempt to separate
745 these brain states through a *brute-force* approach. We observed that the two
746 algorithms tested had a worse discrimination performance in the ELS rats, as
747 verified by the smaller AUC-ROC (*t*-test, for SVM: $t_{(198)} = 99.59$, $p < 0.0001$; for
748 random forest: $t_{(198)} = 107.6$, $p < 0.0001$; Fig. 10F). This worse discriminative
749 performance also arises when using random forest algorithm (which presents the
750 best discriminative performance) on the original whole-spectrum high-
751 dimensional variables (*t*-test, for PFC power: $t_{(198)} = 21.34$, $p < 0.0001$; for HPC
752 power: $t_{(198)} = 58.78$, $p < 0.0001$; for coherence: $t_{(198)} = 80.82$, $p < 0.0001$; for all
753 the spectral estimates combined: $t_{(198)} = 39.23$, $p < 0.0001$; Fig. 10G). This lack
754 of discriminative performance once again corroborates spectral similarities
755 between REM and ACT states in ELS rats.
756
757 **ELS rats present behavioral and neurochemical sensitivity to dopaminergic**
758 **activation**
759 REM-like neural oscillations during the awake state were described in
760 pharmacological and genetic animal models of hyperdopaminergia (Dzirasa et
761 al., 2006). In this context, we conducted a final experiment to investigate the
762 susceptibility of ELS rats to dopaminergic activation using apomorphine
763 (unspecific dopaminergic agonist). We examined behavioral sensitivity by
764 comparing the locomotion produced by apomorphine in the open field (Fig. 11A).
765 Our data demonstrate that apomorphine produces a higher increase in
766 locomotion in ELS rats when compared to CTRL across time blocks (Two-way
767 RM ANOVA, treatment effect: $F_{(1,27)} = 4.260$, $p = 0.0487$, Sidak's *post-hoc:* 5
768 min $p = 0.0376$; Fig. 11B) or between average normalized distances (Mann-
769 Whitney, *n(CTRL, ELS)* = 14/15, $U = 32$, $p = 0.0009$; Fig. 11B inset).
770 Immediately after the behavioral test, we collected samples of NAc, PFC,
771 and HPC to quantify neurotransmitters. The NAc was included in this analysis
772 because it is highly implicated in dopamine sensitivity and exploratory behavior
773 (Salomone et al., 2012). Our data demonstrate that apomorphine reduces
774 dopamine in the NAc of ELS rats, with no effects on dopamine turnover, as
775 measured by DOPAC/DA ratio (Sidak's multiple correction procedure, $t_{(12)} =$
776 3.656, $p = 0.0033$; Fig. 11C). Still, a GLM model implicated NAc dopamine

turnover as a significant predictor of apomorphine-induced hyperlocomotion (*coefficient* = -0.7108*, p* = 0.00297*;* Fig. 11D). Consistently, apomorphine is known to reduce endogenous DA release and DA metabolism in rodents and humans (De La Fuente-Fernández et al., 2001; Ozaki et al., 1989). We also observed a reduction in dopamine turnover in the HPC of ELS rats (Sidak‘s multiple correction procedure, $U = 9$*, p* = 0.0164; Fig. 11E) but no significant effects in the PFC.

Interestingly, we found that the HPC of ELS rats shows a higher Glu content and higher Glu/GABA ratio than CTRL animals following apomorphine injection (Sidak's multiple correction procedure, Glu: $t_{(15)} = 2.566$*, p* = 0.0215; Glu/GABA: $U = 9$*, p* = 0.0079; Fig. 12F) indicating possible disturbances in the excitation/inhibition balance.

HPC-PFC oscillatory dynamics discriminate ELS individuals

After identifying the relevance of specific electrophysiological variables throughout the study, we sought to investigate if collective patterns of the electrophysiological covariates across individuals could assemble a multidimensional oscillatory signature that distinguishes the ELS subjects. Based on relevance, particularity, and state specificity, for this investigation, we chose: (1) HPC theta power (Fig. 7H), (2) theta coherence entropy (Fig. 9J), (3) PFC exponent (Fig. 8G), (4) PFC theta-gamma correlation (Fig. 8C), (5) theta coherence (Fig. 9D), and (6) state map distance (Fig. 10D). By performing PCA, we observed that the first two principal components completely discriminated ELS from CTRL animals (Fig. 12A). This discrimination was further confirmed by fitting a linear discriminant classifier (traces on Fig. 12A) that achieved a 100% accuracy using the entire dataset and 80% accuracy on leave-one-out cross-validation.

Furthermore, unsupervised clustering almost completely discriminated ELS from CTRL rats dividing all the animals into two major clusters: a predominantly ELS cluster (81.82% of ELS animals) and a complete CTRL cluster (100% of CTRL animals; Fig. 12B). The hierarchical clustering approach evidenced a progression of ELS-related oscillatory alterations, with a subcluster presenting an overlap between ELS and CTRL but the other with a more pronounced abnormal spectral fingerprint (Fig. 12B). In addition, the values of

each variable are distinct in each group, which demonstrates that the electrophysiological variables used here are jointly affected by ELS at the functional level. Finally, we show that all the single electrophysiological variables have a high discriminative value (AUC > 0.7) (Fig. 12D), yet, their multivariate linear combination represented by PC1 scores (Fig. 12A) has the best classification performance with an AUC of 1.

Discussion

Here we showed that although ELS does not induce significant neuronal death, it leads to long-term cognitive impairments and behavioral abnormalities. These effects are correlated with neuronal inflammation, hypersensitive dopaminergic neurotransmission, and aberrant HPC-PFC synaptic plasticity. We also found that ELS rats exhibit brain state-dependent alterations – particularly during active behavior and REM sleep – characterized by increased theta power and impaired coordination of local and long-range activity. In addition, ELS presents an abnormal oscillatory state during active behavior oddly similar to REM sleep. Finally, the collective pattern of oscillatory alterations accurately distinguishes ELS from control animals.

Common pathophysiological mechanisms underlying ELS consequences and psychiatric-like impairments

Remarkably, the behavioral alterations found here are well-established translational features of neurodevelopmental disorders and psychiatric disorders related to epilepsy. Studies usually describe increased locomotion (Kubová and Mareš, 2013) and working memory deficits (Tsai et al., 2012) as consequences of ELS. In addition, we also found a reduced PPI, which is less studied but represents a well-established correlate of positive symptoms in clinical psychosis and sensorimotor alterations of ASD (Cheng et al., 2018; Turetsky et al., 2007; Ziermans et al., 2011). Here, we presented a multivariate *sensorimotor factor* comprising a collection of behaviors frequently reported in animal models of schizophrenia, ADHD, and ASD (Ey et al., 2011; Regan et al., 2022; Sigurdsson, 2016). Furthermore, we presented a *cognitive factor* mainly representing working memory deficits, a hallmark in several neurodevelopmental models and psychiatric comorbidities, particularly schizophrenia (Cope et al., 2016).

845 Importantly, the two factors were uncorrelated, but both resulted from ELS. This
846 lack of association between cognitive and sensorimotor impairments suggests
847 two neurobiological substrates, which are confirmed by our multivariate analysis,
848 indicating the association of LTP to cognitive deficits and neuroinflammation to
849 sensorimotor alterations.

850 Surprisingly, we found that cognitive impairment was associated with an
851 abnormally increased susceptibility of HPC-PFC circuits to undergo LTP. This
852 appears to be in contrast with previous studies, which reported reduced
853 hippocampal LTP and cognitive deficits after ELS (Chang et al., 2003; O'Leary et
854 al., 2016). However, no hyperexcitability or spontaneous seizures were described
855 in these studies (O'Leary et al., 2016). In turn, Notenboom et al. (2010) used an
856 animal model of febrile ELS and demonstrated increased LTP in HPC slices
857 related to the reduction of seizure threshold, hyperexcitability, and spontaneous
858 seizures later in life (i.e., epileptogenesis) (Dubé et al., 2006a; Dube et al., 2000).
859 Indeed, paroxysmal activity has been shown to acutely increase synaptic efficacy
860 and hippocampal LTP, thereby reducing the threshold for seizure induction (Ben-
861 Ari & Gho, 1988; Minamiura et al., 1996). In this context, the enhanced LTP
862 observed in our data indicates a relationship with epileptogenesis, which concurs
863 with the epileptiform discharges observed in ELS rats and the increases observed
864 in the hippocampal Glu/GABA ratio.

865 We describe an inverted-U relationship between LTP and working
866 memory, suggesting an optimal level of LTP susceptibility is required for
867 adequate working memory performance. Aberrant synaptic plasticity could be a
868 common mechanism between cognitive deficits and epileptogenesis induced by
869 ELS. Hyperexcitable HPC-PFC circuits could facilitate the spread of epileptiform
870 activity and promote alterations in synaptic saturation and excitatory/inhibitory
871 balance, ultimately leading to cognitive deficits. In this sense, the abnormally
872 increased LTP could impair sensory processes during working memory and
873 explain the poor performance we observed in ELS rats. In a neural network with
874 aberrantly enhanced LTP, synaptic plasticity could be biased toward potentiation,
875 resulting in a lower ability to retain information or adapt to the environment
876 (Navakkode et al., 2022). This rationale is supported by several genetic studies,
877 including on risk genes for neuropsychiatric disorders and autism that described
878 relationships between enhanced LTP and impaired learning (Garcia-Alvarez et

al., 2015; Meng et al., 2002; Nuytens et al., 2013; Yokoi et al., 2015). Interestingly, hyperdopaminergic signaling enhanced HPC-PFC LTP dose-dependently following an "inverted-U" function, where too high or too low dopamine levels disrupted LTP induction, indicating that altered DA neurotransmission could underlie the LTP abnormalities in ELS rats (Goto and Grace, 2006; Otani et al., 2015).

We also report an increase in GFAP expression in ELS animals. Inflammatory processes initiated by a brain insult could lead to functional impairments and, ultimately, psychiatric symptoms (Vezzani et al., 2013). In ELS models, long-term glial activation has been related to behavioral impairments and epileptogenesis (De Oliveira et al., 2008b), while treatment with inflammatory inhibitors resulted in reductions of GFAP and cognitive impairments (Abraham et al., 2012; Somera-Molina et al., 2007). High levels of pro-inflammatory substances and neuroinflammation have been documented in animal models and patients with schizophrenia and ASD (Prata et al., 2017; Vezzani et al., 2013). Noteworthy, the HPC of patients with temporal lobe epilepsy (TLE) and interictal psychosis present greater GFAP and microglia activation than TLE patients without psychosis (Kandratavicius et al., 2015). Additionally, GFAP is elevated in the frontal cortex of autistic subjects (Laurence and Fatemi, 2005). These findings are in accordance with clinical and preclinical biomarkers bridging psychosis and ASD to dopaminergic disturbances resulting from ELS.

In adult SE studies, behavioral abnormalities and cognitive deficits have been positively correlated to neuronal loss and spontaneous seizure frequency (Wolf et al., 2016). It is suggested that the etiological mechanisms of neuropsychiatric-related alterations and epileptic excitability spread progressively over time. Indeed, the behavioral impairments in ELS models tend to be more subtle than in animal models of TLE or hyperdopaminergia. It is possible that the observed alterations in neuroinflammation, neuronal dynamics, and neurochemistry represent initial epileptogenic pathological mechanisms that could progress to spontaneous seizures, progressive neuronal loss, and more intense behavioral manifestations (Dubé et al., 2006b; Kubová and Mareš, 2013).

Dysfunctional patterns of HPC-PFC oscillatory dynamics

Our results demonstrate a locomotion-unrelated increase in HPC theta power during active behavior in ELS animals. Theta oscillations underlie various cognitive processes and are believed to serve as a temporal organizer for multiple functions, such as sensorimotor integration (Buzsáki and Moser, 2013). However, increases in HPC theta power are also observed in hyperdopaminergic-like states, such as following the administration of ketamine or a dopaminergic agonist (Caixeta et al., 2013; Thörn et al., 2022). Increases in theta power are reported in most studies in patients with schizophrenia (Newson and Thiagarajan, 2019) and have been correlated with poor cognitive performance (Curic et al., 2021). Thus, stronger HPC theta power does not necessarily reflect an optimal cognitive state. In fact, abnormal and increased theta power has been described as a consequence of ELS in different models and related to cognitive impairment (Kleen et al., 2011; Velasquez et al., 2023).

Here we observed lower theta-gamma correlations in the PFC of ELS animals, suggesting a disconnection between theta power and local coordination of PFC activity. Similarly, the prolonged febrile model of ELS also presents decreased coordination of gamma activity in the hippocampal circuits (Kloc et al., 2023). In addition, we also observed a flatter PFC power spectrum in ELS animals compared to the normal tilt of CTRL, which has been discussed to indicate excitation/inhibition imbalance (Gao et al., 2017). These findings occurring during active behavior could explain the cognitive-behavioral alterations we observed, at least to some extent.

Desynchronization between limbic-frontal circuits is also reflected by reduced theta coherence during REM. Genetic and neurodevelopmental models of cognitive disorders exhibit a decrease in HPC-PFC theta synchrony correlated with poor spatial working memory performance and anxiety behaviors (Cunniff et al., 2020; Sigurdsson, 2016; Sigurdsson and Duvarci, 2016). Interestingly, increased HPC-PFC theta coherence was described in a model of repetitive ELS (Holmes et al., 2015; Mouchati et al., 2019). Specifically, this enhanced coherence was observed during cognitive performance and associated with a mechanism of neuronal compensation (Kleen et al., 2011; Niedecker et al., 2021). However, during REM sleep, these studies reported a decreased coherence and phase-locking value, indicating different synchronization dynamics depending on the brain state (Niedecker et al., 2021). Here, we observed impaired theta

946 coherence only during REM sleep, which is the brain state with the expected
947 highest coherence values, indicating that ELS animals could not reach or
948 maintain this connectivity at the same maximum capacity as CTRL animals. The
949 results from oscillatory dynamics in the HPC-PFC circuit indicate persistent state-
950 dependent abnormalities in the temporal organization and interaction of local
951 circuits that can contribute to long-term behavioral alterations and cognitive
952 deficits. Further exploration should investigate HPC-PFC coordination during
953 specific cognitive demands, such as working memory tasks, which we have
954 shown to be impaired following ELS.

955 Our results also demonstrated that during ACT behavior, frontal-limbic
956 oscillatory dynamics of ELS rats are unusually similar to REM sleep. Importantly,
957 this finding could not be explained by altered locomotion or sleep architecture.
958 This aberrant active state was more pronounced in the initial 12 h of recording,
959 corresponding to the habituation to the novel environment. Dzirasa et al. (2006)
960 found similar results when recording hyperdopaminergic mice. The authors
961 described a REM-like awake state in DAT-KO mice and wild-type mice injected
962 with amphetamine. Similar to our results, the hyperdopaminergic wake state was
963 marked by a significant increase in hippocampal theta oscillations. Additionally,
964 treatment with antipsychotics reduced these REM-like hippocampal oscillations
965 (Dzirasa et al., 2006). Our similar findings on a developmental model resulting in
966 a psychotic-like phenotype support the relevance of intraindividual REM-wake
967 similarity as a neural mechanism of psychosis. These results also advance
968 previous studies, suggesting a shared involvement of dopamine in the impaired
969 regulation of state-dependent global network dynamics in animal models of
970 psychosis and epilepsy. Also interestingly, it is speculated that REM-wake
971 similarity may represent a neural correlate of oneiric intrusion onto awake
972 consciousness (Dzirasa et al., 2006), which, in the clinical context, could underlie
973 potential phenomenological manifestations of sensorimotor disturbances of
974 neurodevelopmental or psychiatric disorders.

975 In support of these dopaminergic alterations, we showed that ELS
976 promotes apomorphine hypersensitivity and alterations in dopamine
977 neurotransmission. Apomorphine sensitivity has been associated with reduced
978 PPI, hyperlocomotion, and increased NAc dopamine release (Ellenbroek and
979 Cools, 2002). Corroborating our data, neonatal SE promotes amphetamine

980 sensitization and affects both dopaminergic and glutamatergic levels in
981 prefrontal-striatal circuits (Lin et al., 2009). Importantly, alterations in dopamine
982 signaling have been implicated in schizophrenia, ASD, and ADHD (Grace, 2016;
983 Kollins and Adcock, 2014; Kosillo and Bateup, 2021). These results point to
984 enhanced dopaminergic neurotransmission as a potential mechanism underlying
985 the functional abnormalities observed in ELS rats.

986 In conclusion, we describe a comprehensive set of behavioral and
987 neurobiological alterations following ELS that represent common patterns of
988 dysfunctional circuit dynamics between developmental brain disturbances and
989 multiple comorbidities associated. Although further studies should investigate
990 causal links between neurobiological and behavioral alterations, our findings
991 integrate a prominent theory about the pathogenesis of psychiatric symptoms that
992 links stressful insults during development to increased HPC excitability, which
993 would culminate in the hyperactivation of the mesolimbic system, resulting in
994 behavioral dysfunctions (Gomes et al., 2020). Our results add depth to this theory
995 by finding relationships among (1) neurodevelopmental insult, (2)
996 neuroinflammation, (3) hyperexcitable HPC, (4) increased DA drive, (5) disrupted
997 information flow in limbic-frontal circuits, and (6) psychiatric-relevant behaviors.
998 Given the common pathophysiological and behavioral traits linking
999 epileptogenesis and behavioral-cognitive comorbidities, we emphasize the
1000 experimental model's validity to investigate the neurobiological mechanisms of
1001 how an injury during development can lead to neuropsychiatric symptoms. Our
1002 study also demonstrates the potential of a multilevel strategy combining
1003 electrophysiology, behavior, immunohistochemistry, and neurochemistry in
1004 revealing integrated multidimensional mechanisms linking developmental
1005 impacts to epilepsy, cognition, and psychiatric symptoms.

1006

1007 **References**

1008 Abraham J, Fox PD, Condello C, Bartolini A, Koh S. 2012. Minocycline attenuates
1009 microglia activation and blocks the long-term epileptogenic effects of early-
1010 life seizures. *Neurobiol Dis* **46**:425–430. doi:10.1016/j.nbd.2012.02.006

1011 Baram TZ, Eghbal-Ahmadi M, Bender RA. 2002. Is neuronal death required for
1012 seizure-induced epileptogenesis in the immature brain?Progress in Brain
1013 Research. Elsevier. pp. 365–375. doi:10.1016/S0079-6123(02)35033-7

1014 Barr DJ, Levy R, Scheepers C, Tily HJ. 2013. Random effects structure for
1015 confirmatory hypothesis testing: Keep it maximal. *J Mem Lang* **68**:255–278.
1016 doi:10.1016/j.jml.2012.11.001

1017 Barry J, Mahoney J, Holmes G. 2020. Coordination of Hippocampal Theta and
1018 Gamma Oscillations Relative to Spatial Active Avoidance Reflects Cognitive
1019 Outcome After Febrile Status Epilepticus. *Behavioral Neuroscience* **134**:562–
1020 576. doi:10.1037/bne0000388.supp

1021 Ben-Ari Y and, Gho M. 1988. LONG-LASTING MODIFICATION OF THE
1022 SYNAPTIC PROPERTIES OF RAT CA3 HIPPOCAMPAL NEURONES
1023 INDUCED BY KAINIC ACID, Journal of Physiology.

1024 Brunquell PJ, Glennon CM, DiMario FJ, Lerer T, Eisenfeld L. 2002. Prediction of
1025 outcome based on clinical seizure type in newborn infants. *Journal of*
1026 *Pediatrics* **140**:707–712. doi:10.1067/mpd.2002.124773

1027 Bueno-Junior LS, Peixoto-Santos JE, Ruggiero RN, Ávila MAV, Marques DB,
1028 Lopes-Aguiar C, Leite JP. 2018. Interaction between hippocampal-prefrontal
1029 plasticity and thalamic-prefrontal activity. *Sci Rep* **8**. doi:10.1038/s41598-
1030 018-19540-6

1031 Bueno-Junior LS, Ruggiero RN, Rossignoli MT, Del Bel EA, Leite JP, Uchitel OD.
1032 2017. Acetazolamide potentiates the afferent drive to prefrontal cortex
1033 in vivo. *Physiol Rep* **5**. doi:10.14814/phy2.13066

1034 Buzsáki G, Moser EI. 2013. Memory, navigation and theta rhythm in the
1035 hippocampal-entorhinal system. *Nat Neurosci*. doi:10.1038/nn.3304

1036 Caixeta F V., Cornélio AM, Scheffer-Teixeira R, Ribeiro S, Tort ABL. 2013.
1037 Ketamine alters oscillatory coupling in the hippocampus. *Sci Rep* **3**.
1038 doi:10.1038/srep02348

1039 Castelhano ASS, Cassane G dos ST, Scorza FA, Cysneiros RM. 2013. Altered
1040 anxiety-related and abnormal social behaviors in rats exposed to early life
1041 seizures. *Front Behav Neurosci*. doi:10.3389/fnbeh.2013.00036

1042 Castro-Neto EF de, Cunha RH da, Silveira DX da, Yonamine M, Gouveia TLF,
1043 Cavalheiro EA, Amado D, Naffah-Mazzacoratti M da G. 2013. Changes in
1044 aminoacidergic and monoaminergic neurotransmission in the hippocampus
1045 and amygdala of rats after ayahuasca ingestion. *World J Biol Chem* **4**:141.
1046 doi:10.4331/wjbc.v4.i4.141

1047 Chang Y-C, Huang A-M, Kuo Y-M, Wang S-T, Chang Y-Y, Huang C-C. 2003.
1048 Febrile Seizures Impair Memory and cAMP Response-Element Binding
1049 Protein Activation.

1050 Cheng CH, Chan PYS, Hsu SC, Liu CY. 2018. Meta-analysis of sensorimotor
1051 gating in patients with autism spectrum disorders. *Psychiatry Res* **262**:413–
1052 419. doi:10.1016/j.psychres.2017.09.016

1053 Cope ZA, Powell SB, Young JW. 2016. Modeling neurodevelopmental cognitive
1054 deficits in tasks with cross-species translational validity. *Genes Brain Behav*.
1055 doi:10.1111/gbb.12268

1056 Cunniff MM, Markenscoff-Papadimitriou E, Ostrowski J, Rubenstein JLR, Sohal
1057 VS. 2020. Altered hippocampal-prefrontal communication during anxiety-
1058 related avoidance in mice deficient for the autism-associated gene pogz. *Elife*
1059 **9**:1–27. doi:10.7554/eLife.54835

1060 Curic S, Andreou C, Nolte G, Steinmann S, Thiebes S, Polomac N, Haaf M, Rauh
1061 J, Leicht G, Mulert C. 2021. Ketamine Alters Functional Gamma and Theta
1062 Resting-State Connectivity in Healthy Humans: Implications for
1063 Schizophrenia Treatment Targeting the Glutamate System. *Front Psychiatry*
1064 **12**. doi:10.3389/fpsyt.2021.671007

1065 De La Fuente-Fernández R, Lim AS, Sossi V, Holden JE, Calne DB, Ruth TJ,
1066 Stoessl AJ. 2001. Apomorphine-Induced Changes in Synaptic Dopamine
1067 Levels: Positron Emission Tomography Evidence for Presynaptic Inhibition.

1068 De Oliveira DL, Fischer A, Jorge RS, Da Silva MC, Leite M, Gonçalves CA,
1069 Quillfeldt JA, Souza DO, E Souza TM, Wofchuk S. 2008a. Effects of early-life
1070 LiCl-Pilocarpine-induced status epilepticus on memory and anxiety in adult
1071 rats are associated with mossy fiber sprouting and elevated CSF S100B
1072 protein. *Epilepsia* **49**:842–852. doi:10.1111/j.1528-1167.2007.01484.x

1073 De Oliveira DL, Fischer A, Jorge RS, Da Silva MC, Leite M, Gonçalves CA,
1074 Quillfeldt JA, Souza DO, E Souza TM, Wofchuk S. 2008b. Effects of early-life
1075 LiCl-Pilocarpine-induced status epilepticus on memory and anxiety in adult
1076 rats are associated with mossy fiber sprouting and elevated CSF S100B
1077 protein. *Epilepsia* **49**:842–852. doi:10.1111/j.1528-1167.2007.01484.x

1078 Donoghue T, Haller M, Peterson EJ, Varma P, Sebastian P, Gao R, Noto T, Lara
1079 AH, Wallis JD, Knight RT, Shestyuk A, Voytek B. 2020. Parameterizing neural
1080 power spectra into periodic and aperiodic components. *Nat Neurosci*
1081 **23**:1655–1665. doi:10.1038/s41593-020-00744-x

1082 Dreier JW, Pedersen CB, Cotsapas C, Christensen J. 2019. Childhood seizures
1083 and risk of psychiatric disorders in adolescence and early adulthood: a
1084 Danish nationwide cohort study. *Lancet Child Adolesc Health* **3**:99–108.
1085 doi:10.1016/S2352-4642(18)30351-1

1086 Dube C, Chen K, Eghbal-Ahmadi M, Brunson K, Soltesz I, Baram TZ. 2000.
1087 Prolonged Febrile Seizures in the Immature Rat Model Enhance
1088 Hippocampal Excitability Long Term, Ann Neurol.

1089 Dubé C, Richichi C, Bender RA, Chung G, Litt B, Baram TZ. 2006a. Temporal
1090 lobe epilepsy after experimental prolonged febrile seizures: Prospective
1091 analysis. *Brain* **129**:911–922. doi:10.1093/brain/awl018

1092 Dubé C, Richichi C, Bender RA, Chung G, Litt B, Baram TZ. 2006b. Temporal
1093 lobe epilepsy after experimental prolonged febrile seizures: Prospective
1094 analysis. *Brain* **129**:911–922. doi:10.1093/brain/awl018

1095 Dzirasa K, Ribeiro S, Costa R, Santos LM, Lin SC, Grosmark A, Sotnikova TD,
1096 Gainetdinov RR, Caron MG, Nicolelis MAL. 2006. Dopaminergic control of
1097 sleep-wake states. *Journal of Neuroscience* **26**:10577–10589.
1098 doi:10.1523/JNEUROSCI.1767-06.2006

1099 Ellenbroek BA, Cools AR. 2002. Apomorphine Susceptibility and Animal Models
1100 for Psychopathology: Genes and Environment, Behavior Genetics.

1101 Ey E, Leblond CS, Bourgeron T. 2011. Behavioral profiles of mouse models for
1102 autism spectrum disorders. *Autism Research*. doi:10.1002/aur.175

1103 Floresco SB, Seamans JK, Phillips AG. 1997. Selective Roles for Hippocampal,
1104 Prefrontal Cortical, and Ventral Striatal Circuits in Radial-Arm Maze Tasks
1105 With or Without a Delay.

1106 Gao R, Peterson EJ, Voytek B. 2017. Inferring synaptic excitation/inhibition
1107 balance from field potentials. *Neuroimage* **158**:70–78.
1108 doi:10.1016/j.neuroimage.2017.06.078

1109 Garcia-Alvarez G, Shetty MS, Lu B, Yap KAF, Oh-Hora M, Sajikumar S, Bichler
1110 Z, Fivaz M. 2015. Impaired spatial memory and enhanced long-term
1111 potentiation in mice with forebrain-specific ablation of the Stim genes. *Front*
1112 *Behav Neurosci* **9**. doi:10.3389/fnbeh.2015.00180

1113 Gervasoni D, Lin SC, Ribeiro S, Soares ES, Pantoja J, Nicolelis MAL. 2004.
1114 Global forebrain dynamics predict rat behavioral states and their transitions.
1115 *Journal of Neuroscience* **24**:11137–11147. doi:10.1523/JNEUROSCI.3524-
1116 04.2004

1117 Goto Y, Grace AA. 2006. Alterations in Medial Prefrontal Cortical Activity and
1118 Plasticity in Rats with Disruption of Cortical Development. *Biol Psychiatry*
1119 **60**:1259–1267. doi:10.1016/j.biopsych.2006.05.046

1120 Grace AA. 2016. Dysregulation of the dopamine system in the pathophysiology
1121 of schizophrenia and depression. *Nat Rev Neurosci*.
1122 doi:10.1038/nrn.2016.57

1123 Holmes GL. 2016. Effect of Seizures on the Developing Brain and Cognition.
1124 *Semin Pediatr Neurol*. doi:10.1016/j.spen.2016.05.001

1125 Holmes GL. 2009. The Long-Term Effects of Neonatal Seizures. *Clin Perinatol*.
1126 doi:10.1016/j.clp.2009.07.012

1127 Holmes GL, Tian C, Hernan AE, Flynn S, Camp D, Barry J. 2015. Alterations in
1128 sociability and functional brain connectivity caused by early-life seizures are
1129 prevented by bumetanide. *Neurobiol Dis* **77**:204–219.
1130 doi:10.1016/j.nbd.2015.02.015

Kandratavicius L, Lopes-Aguiar C, Bueno-Júnior LS, Romcy-Pereira RN, Hallak JEC, Leite JP. 2012a. Comorbidades psiquiátricas na epilepsia do lobo temporal: Possíveis relações entre desordens psicóticas e comprometimento de circuitos límbicos. *Revista Brasileira de Psiquiatria* **34**:454–466. doi:10.1016/j.rbp.2012.04.007

Kandratavicius L, Ruggiero RN, Hallak JE, Garcia-Cairasco N, Leite JP. 2012b. Pathophysiology of mood disorders in temporal lobe epilepsy. *Revista Brasileira de Psiquiatria* **34**:233–259. doi:10.1016/j.rbp.2012.08.003

Kaufmann R, Goldberg-Stern H, Shuper A. 2009. Attention-deficit disorders and epilepsy in childhood: Incidence, causative relations and treatment possibilities. *J Child Neurol*. doi:10.1177/0883073808330165

Kleen JK, Wu EX, Holmes GL, Scott RC, Lenck-Santini PP. 2011. Enhanced oscillatory activity in the hippocampal-prefrontal network is related to short-term memory function after early-life seizures. *Journal of Neuroscience* **31**:15397–15406. doi:10.1523/JNEUROSCI.2196-11.2011

Kloc ML, Chen Y, Daglian JM, Holmes GL, Baram TZ, Barry JM. 2023. Spatial learning impairments and discoordination of entorhinal-hippocampal circuit coding following prolonged febrile seizures. *Hippocampus*. doi:10.1002/hipo.23541

Kollins SH, Adcock RA. 2014. ADHD, altered dopamine neurotransmission, and disrupted reinforcement processes: Implications for smoking and nicotine dependence. *Prog Neuropsychopharmacol Biol Psychiatry*. doi:10.1016/j.pnpbp.2014.02.002

Kosillo P, Bateup HS. 2021. Dopaminergic Dysregulation in Syndromic Autism Spectrum Disorders: Insights From Genetic Mouse Models. *Front Neural Circuits*. doi:10.3389/fncir.2021.700968

Kubová H, Mareš P. 2013. Are morphologic and functional consequences of status epilepticus in infant rats progressive? *Neuroscience* **235**:232–249. doi:10.1016/j.neuroscience.2012.12.055

Kubova H, Mares P, Suchomelova Â L, Ïek GB, Druga R, Pitka A, Nen È. 2004. Status epilepticus in immature rats leads to behavioural and cognitive impairment and epileptogenesis. *Eur J Neurosci* **19**:3255–65. doi:10.1111/j.1460-9568.2004.03410.x

Laurence JA, Fatemi SH. 2005. Glial fibrillary acidic protein is elevated in superior frontal, parietal and cerebellar cortices of autistic subjects. *Cerebellum* **4**:206–210. doi:10.1080/14734220500208846

Lesting J, Daldrup T, Narayanan V, Himpe C, Seidenbecher T, Pape HC. 2013. Directional Theta Coherence in Prefrontal Cortical to Amygdalo-Hippocampal Pathways Signals Fear Extinction. *PLoS One* **8**. doi:10.1371/journal.pone.0077707

1171 Lin TC, Huang LT, Huang YN, Chen GS, Wang JY. 2009. Neonatal status
1172 epilepticus alters prefrontal-striatal circuitry and enhances
1173 methamphetamine-induced behavioral sensitization in adolescence.
1174 *Epilepsy and Behavior* **14**:316–323. doi:10.1016/j.yebeh.2008.12.005

1175 Lopes-Aguiar C, Ruggiero RN, Rossignoli MT, Esteves I de M, Peixoto-Santos
1176 JE, Romcy-Pereira RN, Leite JP. 2020. Long-term potentiation prevents
1177 ketamine-induced aberrant neurophysiological dynamics in the
1178 hippocampus-prefrontal cortex pathway in vivo. *Sci Rep* **10**.
1179 doi:10.1038/s41598-020-63979-5

1180 Marín O. 2016. Developmental timing and critical windows for the treatment of
1181 psychiatric disorders. *Nat Med*. doi:10.1038/nm.4225

1182 Marques DB, Ruggiero RN, Bueno-Junior LS, Rossignoli MT, Leite JP. 2022.
1183 Prediction of Learned Resistance or Helplessness by Hippocampal-
1184 Prefrontal Cortical Network Activity during Stress. *Journal of Neuroscience*
1185 **42**:81–96. doi:10.1523/JNEUROSCI.0128-21.2021

1186 Meng Y, Zhang Y, Tregoubov V, Janus C, Cruz L, Jackson M, Lu W-Y,
1187 Macdonald JF, Wang JY, Falls DL, Jia Z. 2002. Abnormal Spine Morphology
1188 and Enhanced LTP in LIMK-1 Knockout Mice ever, the molecular
1189 mechanisms that regulate the actin cytoskeleton at synapses are poorly
1190 understood. Previous studies in cultured cells have indicated that, Neuron.

1191 Minamiura Y, Hirayama K, Murata R, Matsuura S. 1996. Effect of hyperthermia
1192 on hippocampal synaptic transmission and CA3 kindling in developing rats,
1193 Brain Research.

1194 Mouchati PR, Barry JM, Holmes GL. 2019. Functional brain connectivity in a
1195 rodent seizure model of autistic-like behavior. *Epilepsy and Behavior* **95**:87–
1196 94. doi:10.1016/j.yebeh.2019.03.046

1197 Navakkode S, Zhai J, Wong YP, Li G, Soong TW. 2022. Enhanced long-term
1198 potentiation and impaired learning in mice lacking alternative exon 33 of
1199 CaV1.2 calcium channel. *Transl Psychiatry* **12**. doi:10.1038/s41398-021-
1200 01683-2

1201 Newson JJ, Thiagarajan TC. 2019. EEG Frequency Bands in Psychiatric
1202 Disorders: A Review of Resting State Studies. *Front Hum Neurosci*.
1203 doi:10.3389/fnhum.2018.00521

1204 Niedecker RW, Kloc ML, Holmes GL, Barry JM. 2021. Effects of early life seizures
1205 on coordination of hippocampal–prefrontal networks: Influence of sex and
1206 dynamic brain states. *Epilepsia* **62**:1701–1714. doi:10.1111/epi.16927

1207 Notenboom RGE, Ramakers GMJ, Kamal A, Spruijt BM, De Graan PNE. 2010.
1208 Long-lasting modulation of synaptic plasticity in rat hippocampus after early-
1209 life complex febrile seizures. *European Journal of Neuroscience* **32**:749–758.
1210 doi:10.1111/j.1460-9568.2010.07321.x

1211 Nuytens K, Gantois I, Stijnen P, Iscru E, Laeremans A, Serneels L, Van Eylen L,
1212 Liebhaber SA, Devriendt K, Balschun D, Arckens L, Creemers JWM,
1213 D'Hooge R. 2013. Haploinsufficiency of the autism candidate gene
1214 Neurobeachin induces autism-like behaviors and affects cellular and
1215 molecular processes of synaptic plasticity in mice. *Neurobiol Dis* **51**:144–151.
1216 doi:10.1016/j.nbd.2012.11.004

1217 O'Leary H, Bernard PB, Castano AM, Benke TA. 2016. Enhanced long term
1218 potentiation and decreased AMPA receptor desensitization in the acute
1219 period following a single kainate induced early life seizure. *Neurobiol Dis*
1220 **87**:134–144. doi:10.1016/j.nbd.2015.12.005

1221 Otani S, Bai J, Blot K. 2015. Dopaminergic modulation of synaptic plasticity in rat
1222 prefrontal neurons. *Neurosci Bull*. doi:10.1007/s12264-014-1507-3

1223 Ozaki N, Nakahara T, Miura H, Kasahara Y, Nagatsu S. 1989. Effects of
1224 Apomorphine on In Vivo Release of Dopamine and Its Metabolites in the
1225 Prefrontal Cortex and the Striaturn, Studied by a Microdialysis Method, J.
1226 Neurochem.

1227 Peixoto-Santos JE, Velasco TR, Galvis-Alonso OY, Araujo D, Kandratavicius L,
1228 Assirati JA, Carlotti CG, Scandiuzzi RC, Dos Santos AC, Leite JP. 2015.
1229 Temporal lobe epilepsy patients with severe hippocampal neuron loss but
1230 normal hippocampal volume: Extracellular matrix molecules are important for
1231 the maintenance of hippocampal volume. *Epilepsia* **56**:1562–1570.
1232 doi:10.1111/epi.13082

1233 Prata J, Santos SG, Almeida MI, Coelho R, Barbosa MA. 2017. Bridging Autism
1234 Spectrum Disorders and Schizophrenia through inflammation and
1235 biomarkers - pre-clinical and clinical investigations. *J Neuroinflammation*.
1236 doi:10.1186/s12974-017-0938-y

1237 Racine RJ. 1971. Electroencephalography and Clinical Neurophysiology
1238 MODIFICATION OF SEIZURE ACTIVITY BY ELECTRICAL STIMULATION:
1239 II. MOTOR SEIZURE. *Electroencephalogr Clin Neurophysiol* **32.**:281–94.

1240 Regan SL, Williams MT, Vorhees C V. 2022. Review of rodent models of attention
1241 deficit hyperactivity disorder. *Neurosci Biobehav Rev*.
1242 doi:10.1016/j.neubiorev.2021.11.041

1243 Rojas DC, Wilson LB. 2014. γ-band abnormalities as markers of autism spectrum
1244 disorders. *Biomark Med*. doi:10.2217/bmm.14.15

1245 Ruggiero RN, Lopes-Aguiar C, Leite JP. 2012. Early Life Seizures and Their
1246 Long-term Impacts on Cognition: The Role of Synaptic Plasticity
1247 Dysfunctions as an Underlying Mechanism. *Journal of epilepsy and clinical*
1248 *neurophysiology.*

1249 Ruggiero RN, Rossignoli MT, Lopes-Aguiar C, Leite JP, Bueno-Junior LS,
1250 Romcy-Pereira RN. 2018. Lithium modulates the muscarinic facilitation of

1251 synaptic plasticity and theta-gamma coupling in the hippocampal-prefrontal
1252 pathway. *Exp Neurol* **304**:90–101. doi:10.1016/j.expneurol.2018.02.011

1253 Ruggiero RN, Rossignoli MT, Marques DB, de Sousa BM, Romcy-Pereira RN,
1254 Lopes-Aguiar C, Leite JP. 2021. Neuromodulation of Hippocampal-Prefrontal
1255 Cortical Synaptic Plasticity and Functional Connectivity: Implications for
1256 Neuropsychiatric Disorders. *Front Cell Neurosci*.
1257 doi:10.3389/fncel.2021.732360

1258 Scott KE, Schormans AL, Pacoli KY, De Oliveira C, Allman BL, Schmid S. 2018.
1259 Altered auditory processing, filtering, and reactivity in the cntnap2 knock-out
1260 rat model for neurodevelopmental disorders. *Journal of Neuroscience*
1261 **38**:8588–8604. doi:10.1523/JNEUROSCI.0759-18.2018

1262 Short AK, Baram TZ. 2019. Early-life adversity and neurological disease: age-old
1263 questions and novel answers. *Nat Rev Neurol*. doi:10.1038/s41582-019-
1264 0246-5

1265 Sigurdsson T. 2016. Neural circuit dysfunction in schizophrenia: Insights from
1266 animal models. *Neuroscience*. doi:10.1016/j.neuroscience.2015.06.059

1267 Sigurdsson T, Duvarci S. 2016. Hippocampal-prefrontal interactions in cognition,
1268 behavior and psychiatric disease. *Front Syst Neurosci*.
1269 doi:10.3389/fnsys.2015.00190

1270 Sinh Y, Raol H, Budreck EC, Brooks-Kayal AR. 2003. Epilepsy after Early-Life
1271 Seizures Can Be Independent of Hippocampal Injury, Ann Neurol.

1272 Somera-Molina KC, Robin B, Somera CA, Anderson C, Stine C, Koh S, Behanna
1273 HA, Van Eldik LJ, Watterson DM, Wainwright MS. 2007. Glial activation links
1274 early-life seizures and long-term neurologic dysfunction: Evidence using a
1275 small molecule inhibitor of proinflammatory cytokine upregulation. *Epilepsia*
1276 **48**:1785–1800. doi:10.1111/j.1528-1167.2007.01135.x

1277 Thörn CW, Kafetzopoulos V, Kocsis B. 2022. Differential Effect of Dopamine D4
1278 Receptor Activation on Low-Frequency Oscillations in the Prefrontal Cortex
1279 and Hippocampus May Bias the Bidirectional Prefrontal–Hippocampal
1280 Coupling. *Int J Mol Sci* **23**. doi:10.3390/ijms231911705

1281 Tsai ML, Crutchley M, Boyce R, Ma J, Boon F, Cain DP, Leung LS. 2012. Long-
1282 lasting auditory gating deficit accompanied by GABA B receptor dysfunction
1283 in the hippocampus after early-life limbic seizures in rats. *Physiol Behav*
1284 **106**:534–541. doi:10.1016/j.physbeh.2012.03.033

1285 Turetsky BI, Calkins ME, Light GA, Olincy A, Radant AD, Swerdlow NR. 2007.
1286 Neurophysiological endophenotypes of schizophrenia: The viability of
1287 selected candidate measures. *Schizophr Bull*. doi:10.1093/schbul/sbl060

1288 Velasquez F, Dickson C, Kloc ML, Schneur CA, Barry JM, Holmes GL. 2023.
1289 Optogenetic modulation of hippocampal oscillations ameliorates spatial
1290 cognition and hippocampal dysrhythmia following early-life seizures.
1291 *Neurobiol Dis* **178**. doi:10.1016/j.nbd.2023.106021

Vezzani A, Aronica E, Mazarati A, Pittman QJ. 2013. Epilepsy and brain inflammation. *Exp Neurol*. doi:10.1016/j.expneurol.2011.09.033

Wolf DC, Bueno-Júnior LS, Lopes-Aguiar C, Do Val Da Silva RA, Kandratavicius L, Leite JP. 2016. The frequency of spontaneous seizures in rats correlates with alterations in sensorimotor gating, spatial working memory, and parvalbumin expression throughout limbic regions. *Neuroscience* **312**:86–98. doi:10.1016/j.neuroscience.2015.11.008

Yokoi F, Chen HX, Dang MT, Cheetham CC, Campbell SL, Roper SN, Sweatt JD, Li Y. 2015. Behavioral and electrophysiological characterization of Dyt1 heterozygous knockout mice. *PLoS One* **10**. doi:10.1371/journal.pone.0120916

Ziermans T, Schothorst P, Magnée M, van Engeland H, Kemner C. 2011. Reduced prepulse inhibition in adolescents at risk for psychosis: A 2-year follow-up study. *Journal of Psychiatry and Neuroscience* **36**:127–134. doi:10.1503/jpn.100063

Figures and Legends

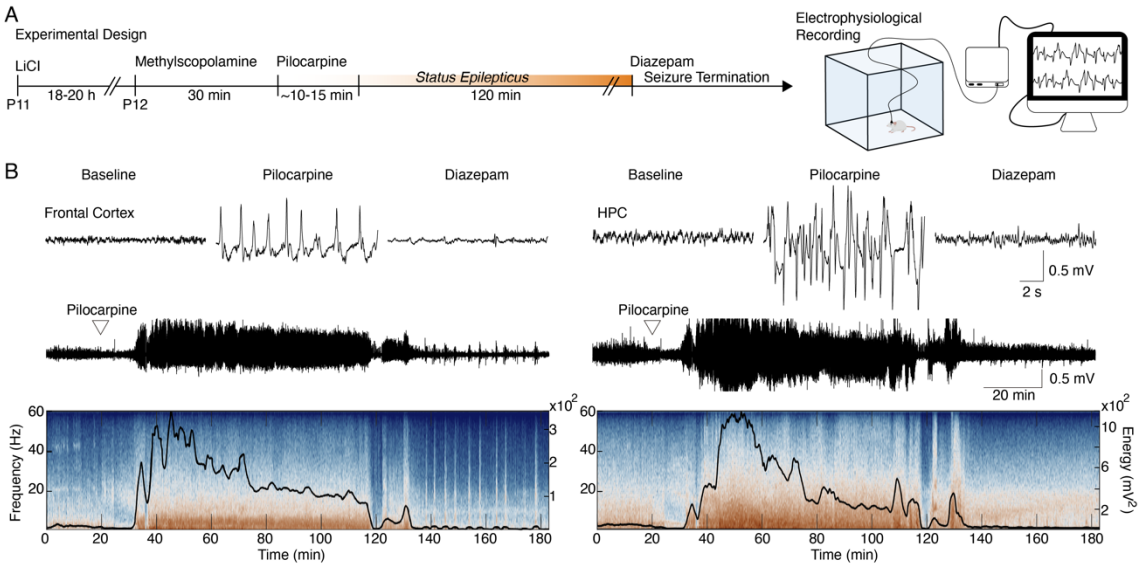

Figure 1. ELS induction. ***A,*** Experimental design representing early-life SE induction and monitoring. ***B,*** Representative traces of LFP during baseline, motor seizure induced by pilocarpine, and ELS interruption with diazepam injection (top). Representative LFP from the frontal cortex and HPC throughout the experiment (middle). LFPs are aligned with their respective spectrograms and energy curves (bottom).

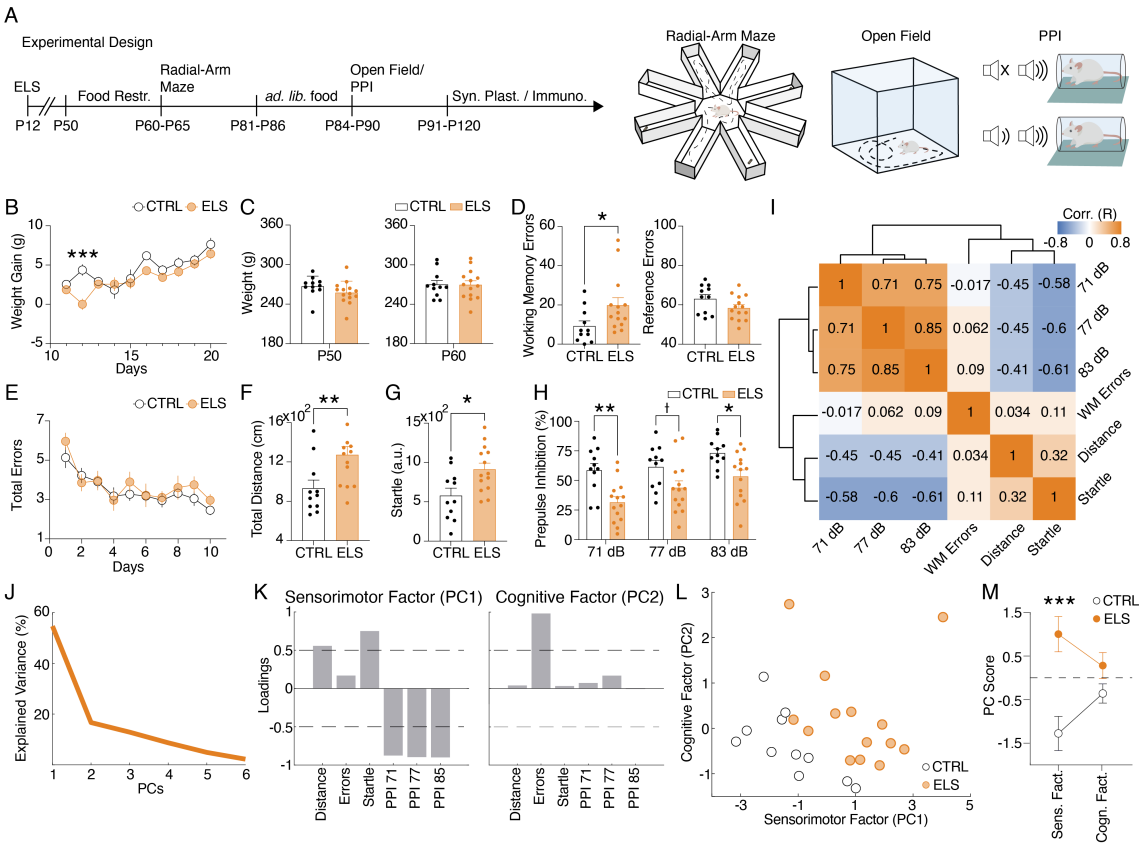

Figure 2. ELS induces cognitive and sensorimotor impairments. *A,* Experimental design representing early-life SE induction, age of the animals during the experiments, and behavioral tests performed. ***B,*** Weight gain after ELS induction. ELS rats showed weight loss only on the ELS induction day. ***C,*** No weight differences between ELS and CTRL throughout experiments in adulthood, regardless if before food restriction (left) or during food restriction (right). ***D,*** Working memory task on the radial-arm maze. ***E,*** ELS rats showed an increase in working memory errors across sessions (left) without differences in the number of reference errors (right). E, ELS rats showed a similar learning curve when compared to CTRL. ***F,*** Hyperlocomotion of ELS rats in the open field test. ***G,*** Higher acoustic startle of ELS rats. ***H,*** Impaired sensorimotor gating in ELS rats as measured in the PPI test with three stimulus intensities. ***I,*** Correlation matrix of all behavioral variables. Note a cluster of positive correlations formed by the PPI measures and another cluster of negative correlations formed by the PPI measures with distance traveled on the open field and the acoustic startle. Working memory errors were not correlated with the other behavioral features. ***J,*** Explained variance from principal components analysis (PCA). Note that the two first PCs explain 71.32% of the data. ***K,*** Loadings of the behavioral variables on each principal component (PC) reveal a *sensorimotor factor* (PC1) and an uncorrelated *cognitive factor* (PC2). ***L,*** PCA of the behavioral features showing each animal projected onto the new factors. ***M,*** The sensorimotor factor distinguishes ELS from CTRL animals, as we compare the PC scores from each group. † $p < 0.1$, *$p < 0.05$, **$p < 0.01$, ***$p < 0.001$. Error bars represent the mean ± SEM.

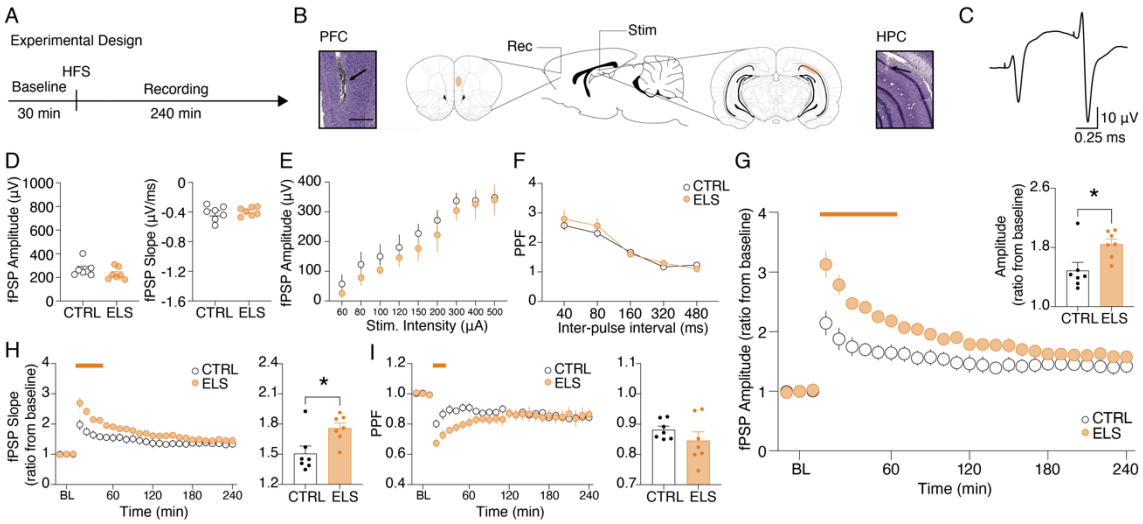

Figure 3. Aberrant HPC-PFC synaptic plasticity in animals submitted to ELS. *A,* Experimental design including high-frequency stimulation (HFS) to LTP induction. ***B,*** Electrode placement and representative electrolytic lesions in Cresyl Violet stained coronal sections. ***C,*** Representative evoked fPSPs in the PFC. No difference between ELS and CTRL rats in terms of basal neurotransmission and synaptic efficacy, as shown by: ***(D)***, fPSP amplitude (left) and slope (right); ***(E),*** input-output curve; and ***(F),*** paired-pulse facilitation (PPF) curve. ***G,*** Despite no changes in basal synaptic efficacy, ELS rats showed aberrantly increased LTP, represented by higher fPSP amplitude ratios from baseline (BL) post-HFS, both across time blocks (main curve graph) and their averages (bar graph, inset). ***H,*** As in ***G,*** but from fPSP slopes. ***I,*** ELS rats showed reduced PPF in the initial 30 min (curve graph). Averaged data resulted in no differences between the groups (bar graph, inset). † $p < 0.1$, *$p < 0.05$, **$p < 0.01$, ***$p < 0.001$. Error bars represent the mean ± SEM.

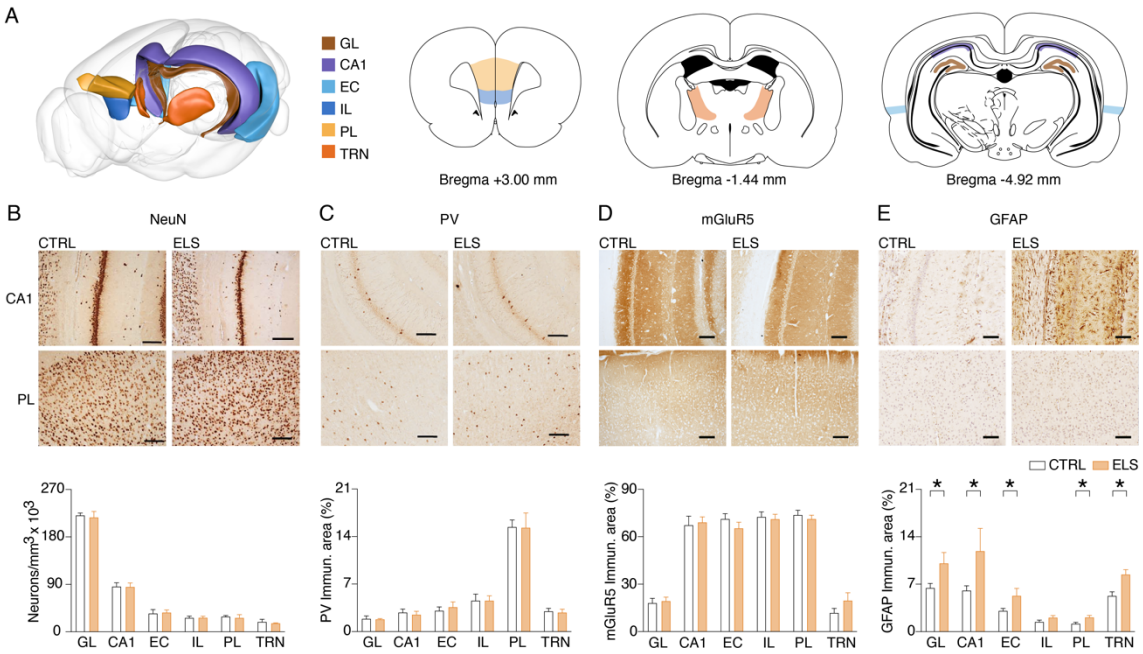

Figure 4. ELS induces long-term neural inflammation, but not neuronal loss. ***A*** 3-D brain diagram and coronal sections representing the brain regions investigated. ***B-E***, Representative photomicrographs from immunohistochemistry each pair of columns represents a group comparison (left CTRL and right ELS) and each line is related to CA1 and PL, respectively. ***B,*** NeuN immunohistochemistry showing that ELS rats did not present neuronal loss. ***C,*** Parvalbumin (PV) immunohistochemistry. ***D,*** mGluR5: ***E***, GFAP, showing increased astrogliosis induced by ELS. GL: Granule layer of dentate gyrus; CA1: *Cornu Ammonis* 1; EC: Entorhinal cortex; IL: Infralimbic cortex; PL: Prelimbic cortex; TRN: Thalamic Reticular Nucleus. *$p < 0.05$ Error bars represent the mean ± SEM.

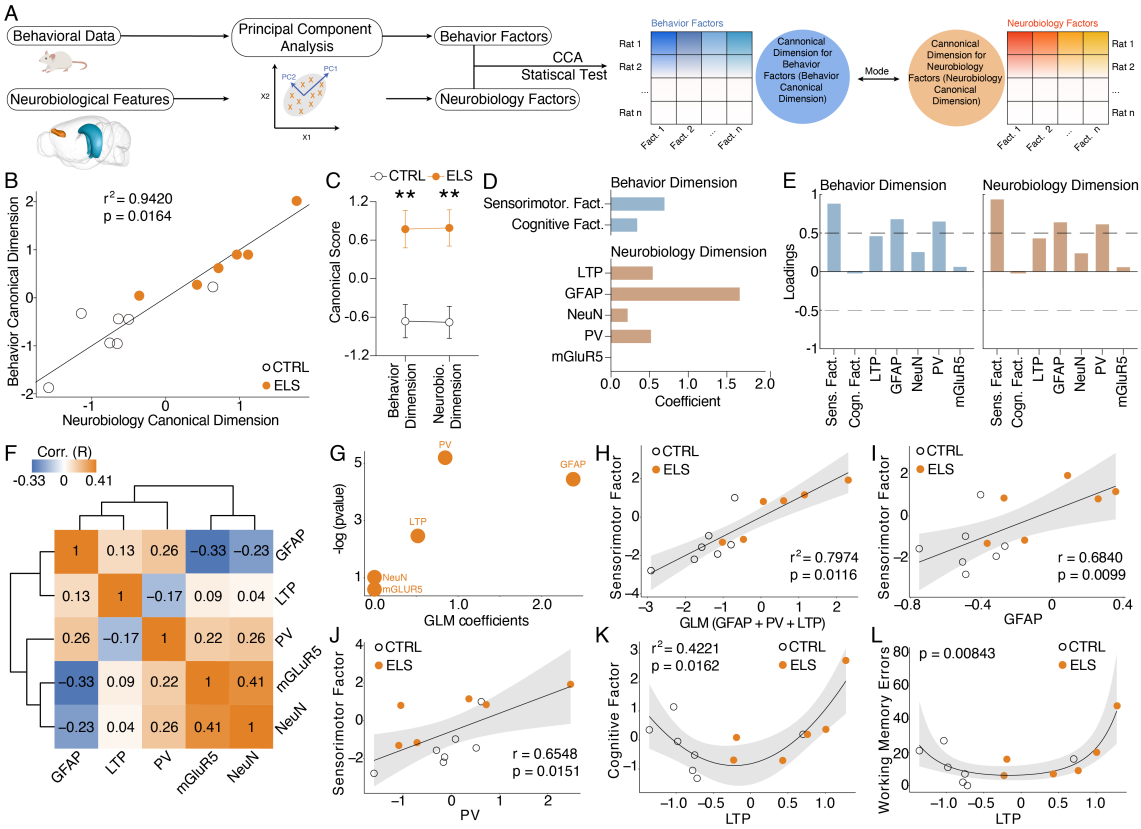

Figure 5. Cognitive impairment and sensorimotor deficits are distinctly correlated with abnormal LTP and neuroinflammation. *A,* Steps performed in data processing and analysis for canonical correlation analysis (CCA). ***B,*** CCA analysis showing CTRL and ELS animals projected onto the first canonical correlation. We found a strong correlation between the neurobiology canonical dimension and the behavior canonical dimension. ***C,*** Canonical scores showing the clear CTRL *vs.* ELS difference that the CCA was able to capture. ***D,*** Coefficients for behavior and neurobiology canonical dimensions, showing greater contributions of the sensorimotor factor, GFAP, PV, and LTP for the correlation. ***E,*** Loadings of the behavioral and neurobiological variables on each canonical correlation dimension indicating an association between GFAP and PV with the sensorimotor factor. ***F,*** Correlation matrix showing only weak correlations between the neurobiological features. ***G,*** GLM regression between neurobiological features and the sensorimotor factor. ***H***, GLM model between neurobiological features and the sensorimotor factor show a strong association with GFAP, PV, and LTP. ***I,*** GLM regression between LTP and the cognitive factor shows a quadratic association (left). This quadratic association was further confirmed performing a quasi-Poisson regression between LTP and raw values of working memory errors (right). **p < 0.01. Error bars represent the mean ± SEM.

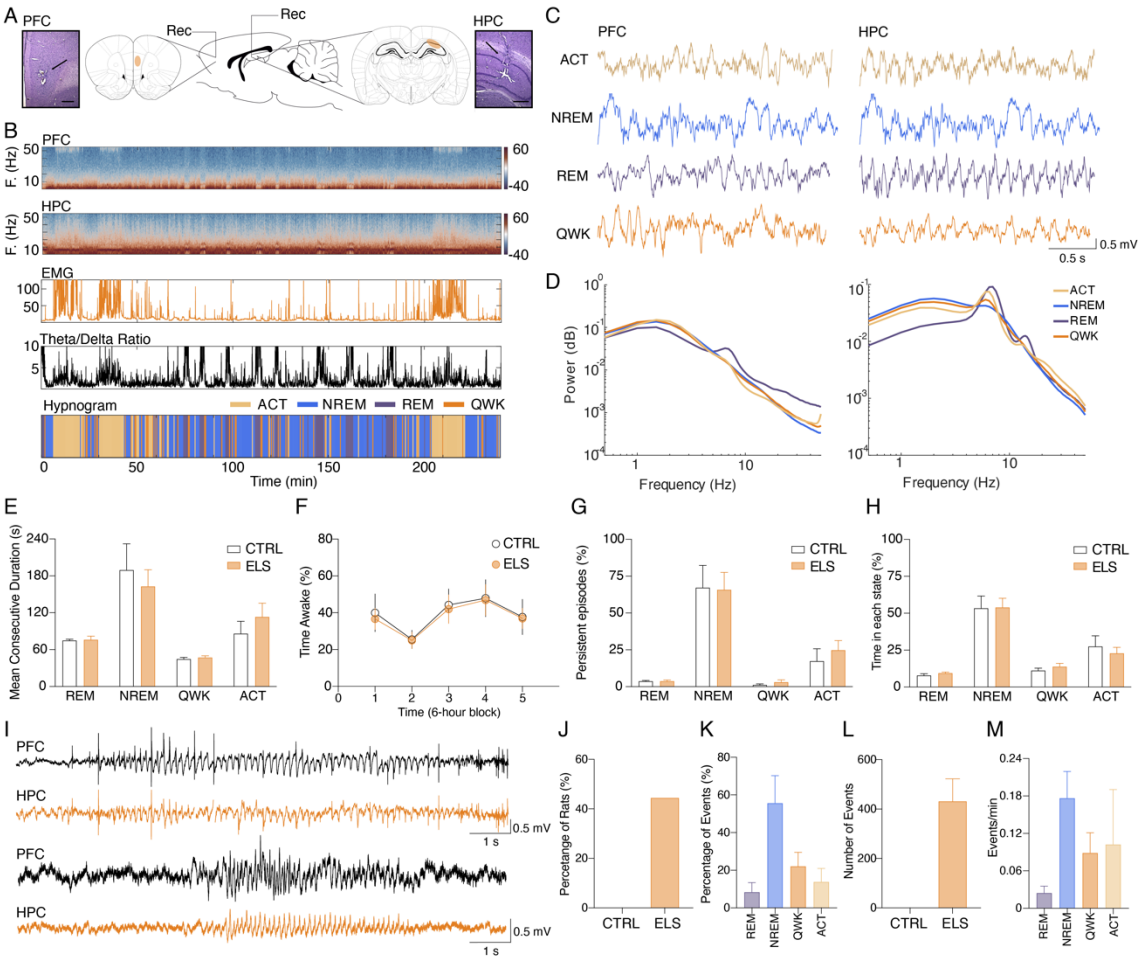

Figure 6. Classification of sleep-wake states and electrographic discharges in ELS rats. *A,* Electrode placement and representative electrolytic lesions in Nissl-stained coronal sections. ***B,*** Representative spectrogram, electromyogram (EMG) root mean squared (RMS), and HPC theta/delta ratio used to score the sleep-wake cycle and to generate the hypnogram (bottom). ***C,*** Representative LFPs (top) recorded from PFC and HPC during ACT, NREM, REM, and QWK. ***D,*** Average power spectral density for each state in the PFC and HPC of a representative CTRL animal. Note the increase in HPC theta power during ACT and REM. ELS rats did not present alterations in the sleep-wake cycle. ***E-H***, There were no differences between ELS and CTRL in the ***(E)*** Mean duration of consecutive epochs for each state, ***(F)*** percentage of time awake across 6-h blocks, and in the ***(G)*** number of persistent episodes (episodes lasting longer than 3 s, top) or the ***(H)*** percentage of time spent in each state (bottom). ***I,*** Representative LFP from PFC and HPC showing a representative spike-wave discharge (SWD, top) and a poly-spike discharge (bottom). ***J,*** Electrographic discharges were found in 44.5% of ELS animals and were absent in CTRL animals. ***K,*** Percentage of events occurring in each sleep-wake stage. ***L,*** Average total number of SWD events in CTRL and ELS animals. ***M,*** Frequency of SWDs occurring per state. SWDs events rarely occurred during REM. Error bars represent the mean ± SEM.

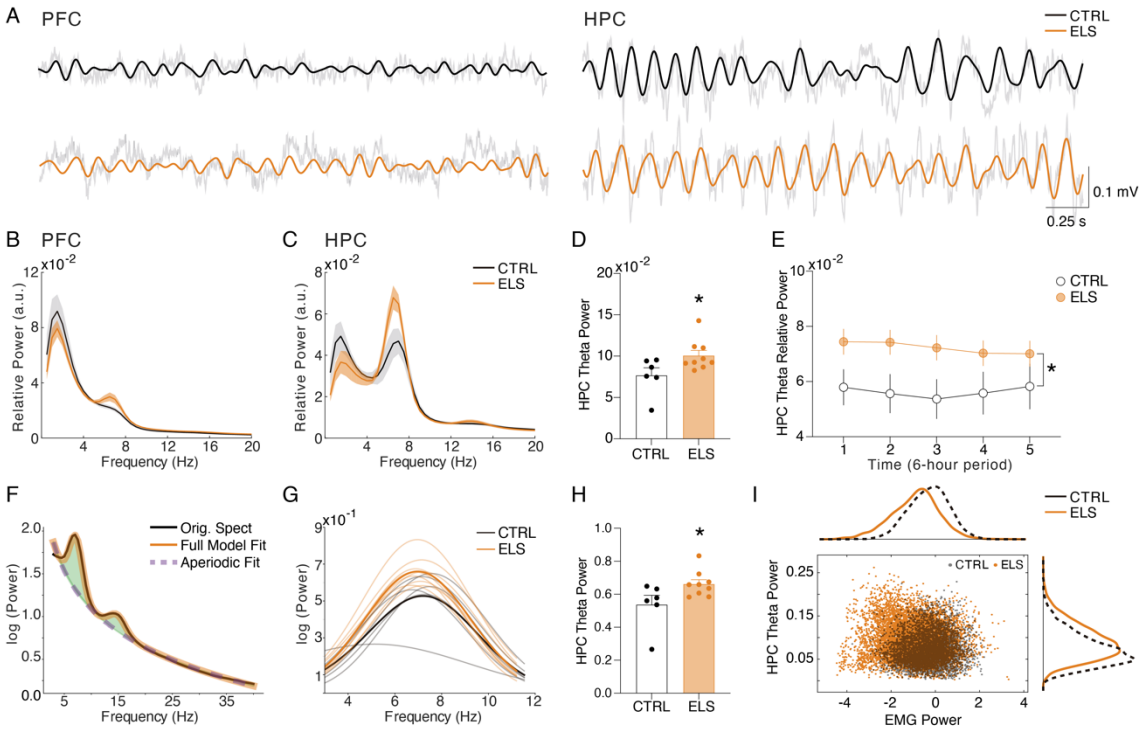

Figure 7. Increased HPC theta power during behavioral activity in ELS animals. *A,* Representative raw LFPs (transparent black lines) and theta-filtered signal of CTRL (black) and ELS (orange) from the PFC (left) and HPC (right) during ACT. ***B,*** Relative PSD of the PFC during ACT. ***C,*** Relative PSD of the HPC during ACT. ***D,*** ELS rats present an enhanced HPC theta power during ACT. ***E,*** Theta relative power during each of the 6-hour periods of recording, showing a general increase in the ELS animals that is more pronounced in the initial 18 h of recording. ***F,*** Parametric model used to distinguish oscillatory from aperiodic component. ***G,*** Oscillatory components extracted from ACT PSDs used to calculate theta power. ***H,*** Theta power increase in ELS rats is due to a true oscillatory component and not from the aperiodic activity in ACT states. ***I,*** Theta power increase in ELS rats is independent of locomotor activity. Note from the distribution of relative theta power and Z-scored EMG (trapezius) values for all rats that EMG power is not related to the regions of greater theta power in the ELS animals. *$p < 0.05$. Error bars represent the mean ± SEM.

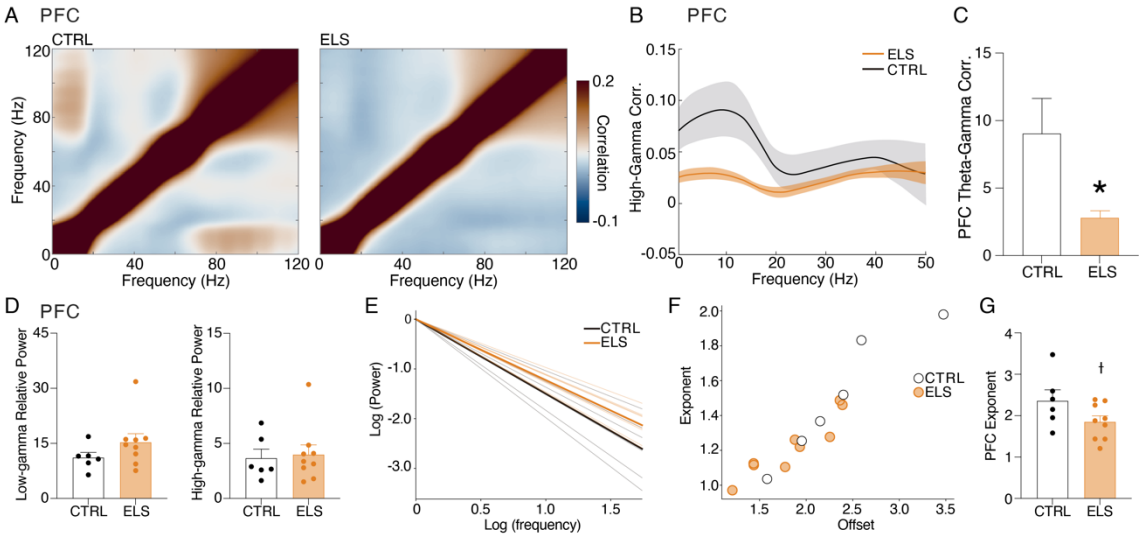

Figure 8. ELS promotes abnormal gamma coordination in the PFC during behavioral activity. ELS rats present an abnormal gamma activity in the PFC. ***A,*** Grand-average amplitude correlogram for CTRL (left) and ELS (right) group. Note the absence of amplitude correlation between theta and gamma activity in the ELS group. ***B,*** High-gamma (65-100 Hz) correlation with low-frequency activity. Note the peak around theta oscillation in the CTRL group and the absence in ELS. ***C,*** ELS present an impaired theta-gamma amplitude correlation. ***D,*** There is no difference between the low- (top) and high-gamma (bottom) average power. ***E,*** Aperiodic activity extracted from the PFC of each rat during ACT state. ***F,*** Distribution of the parameters of the aperiodic component (exponent and offset) for each rat. ***G,*** ELS rats show a tendency to reduction (p = 0.0656) in the exponent parameter of the aperiodic component, as illustrated by the flatter spectra. † $p < 0.1$, *$p < 0.05$. Error bars represent the mean ± SEM.

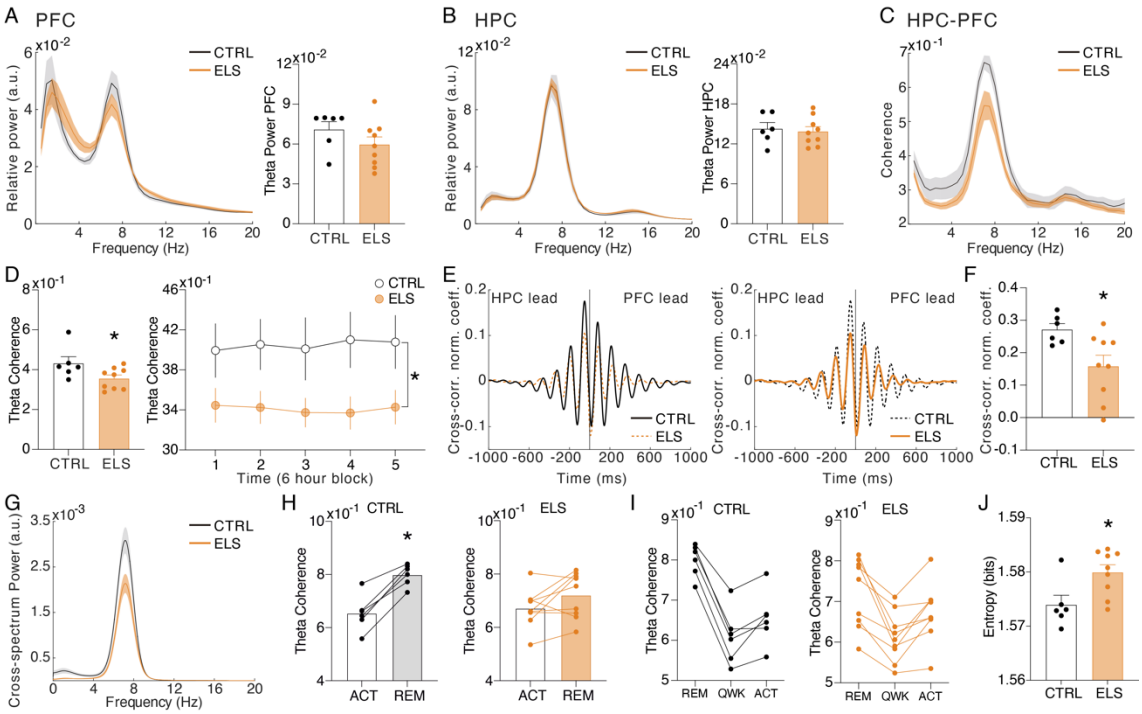

Figure 9. ELS impairs HPC-PFC coherence during REM sleep. *A,* PSD in the PFC during REM. ***B,*** PSD in the HPC during REM. No significant alterations in theta power during REM are observed in ELS rats. ***C,*** Theta coherence is diminished in ELS rats. ***D,*** Significant effect on the HPC-PFC theta coherence by averaging the entire recording (left) and across all periods (right). ***E,*** Time domain cross-correlation between PFC and HPC LFPs during REM epochs highlighting CTRL (left) and ELS (right) group averages. ***F,*** Reduction in the peak of correlation between -80 to -20 ms in ELS rats***. G,*** Average cross-spectrum power density showing a reduced theta peak in the ELS rats. ***H,*** Theta HPC-PFC coherence increases from ACT to REM states. We can observe that all the CTRL rats present an increase from ACT to REM, while in ELS rats this is not observed. Paired *t*-test *p < 0.05. ***I,*** Theta coherence dynamics across the sleep-wake cycle. CTRL rats display a homogeneous dynamics with theta coherence being maximal at REM, minimal in QWK, and intermediate in ACT states. This dynamic is disrupted in ELS rats that display a higher variance between animals, with some animals displaying similar coherence in REM and ACT. ***J,*** Entropy of the theta coherence dynamics is higher in ELS rats, representing the more homogeneous values across states.

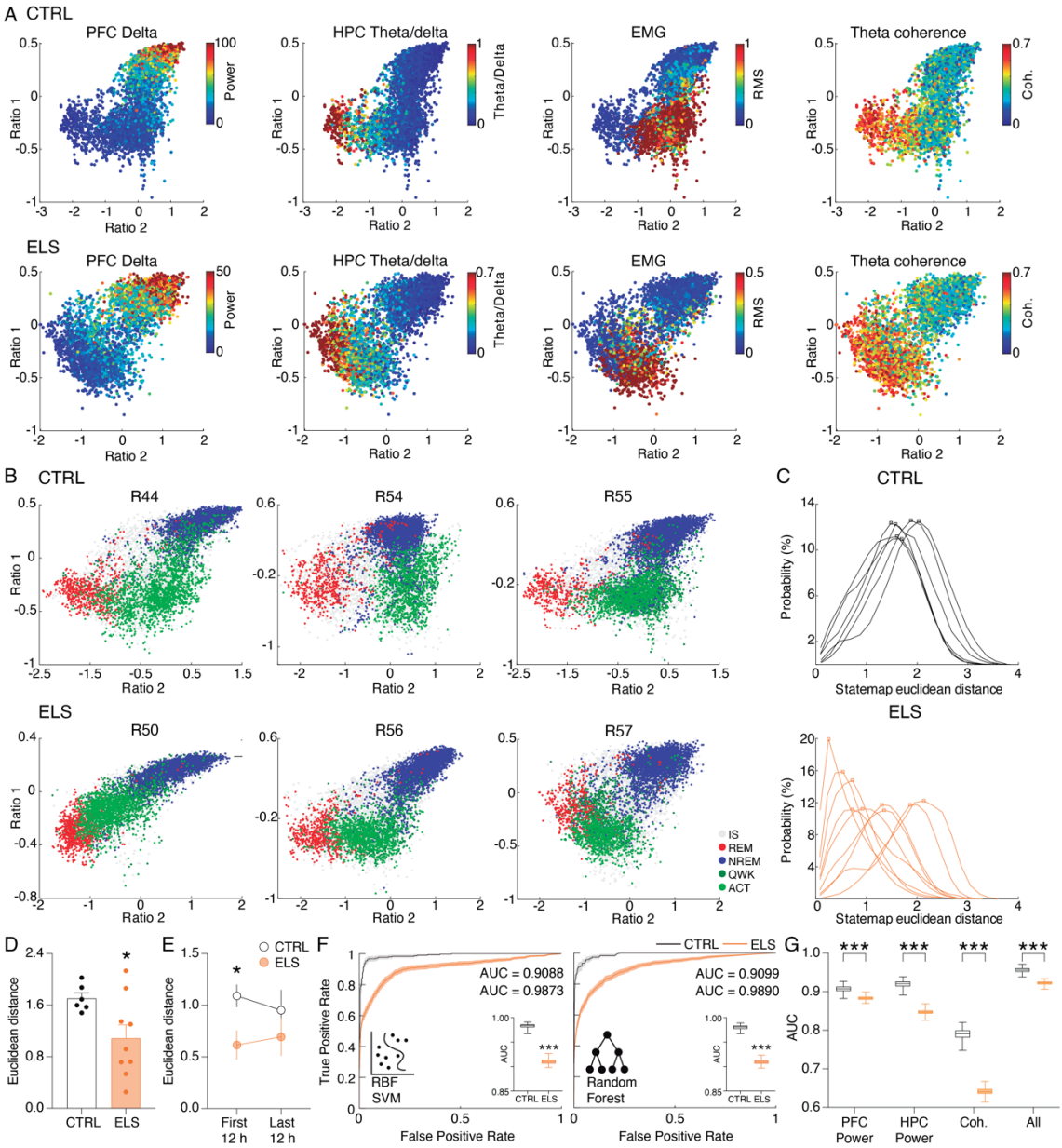

Figure 10. ELS rats display REM-like oscillatory dynamics during active behavior. *A,* State map construction reflects the sleep-wake cycle and spectral dynamics for one representative CTRL (top) and ELS (bottom) rat. PFC delta power is evident during NREM, theta/delta ratio is maximum in REM, EMG power describes ACT states, and HPC-PFC theta coherence is stronger close to REM. Note that in the ELS rat, the coherence is also broadly high during the ACT state. ***B,*** Representative state maps from three CTRL (top) and three ELS (bottom) rats. CTRL rats displayed a clear separation between REM (red), ACT (light green), and NREM (blue) clusters. ELS displayed an overlap between REM and ACT states. ***C,*** Distributions of the Euclidean distances between each REM and ACT epoch for CTRL (top) and ELS (bottom) rats. ELS distributions were heterogeneous, many of which were skewed to shorter distances. ***D,*** Average Euclidean distance showing that ELS rats have REM-like oscillatory dynamics during active behavior. ***E,*** REM-like oscillations during ACT were more pronounced in ELS during the initial 12 h of recording. ***F,*** Machine learning approach to decode REM *versus* ACT states. We used radial

basis function support vector machine (SVM) and random forest (RF) algorithm in order to classify REM and ACT epochs in CTRL (black) or ELS (orange) rats. Using a bootstrapped confidence interval, we observed that the discriminative performance was worse in ELS animals, even when using “brute-force” algorithms. ***G,*** A machine learning algorithm (random forest) fitted on whole-spectrum data also shows a significantly worse performance in ELS for PFC power, HPC power, coherence, and all estimates combined. † $p < 0.1$, *$p < 0.05$, **$p < 0.01$, ***$p < 0.001$. Error bars represent the mean ± SEM.

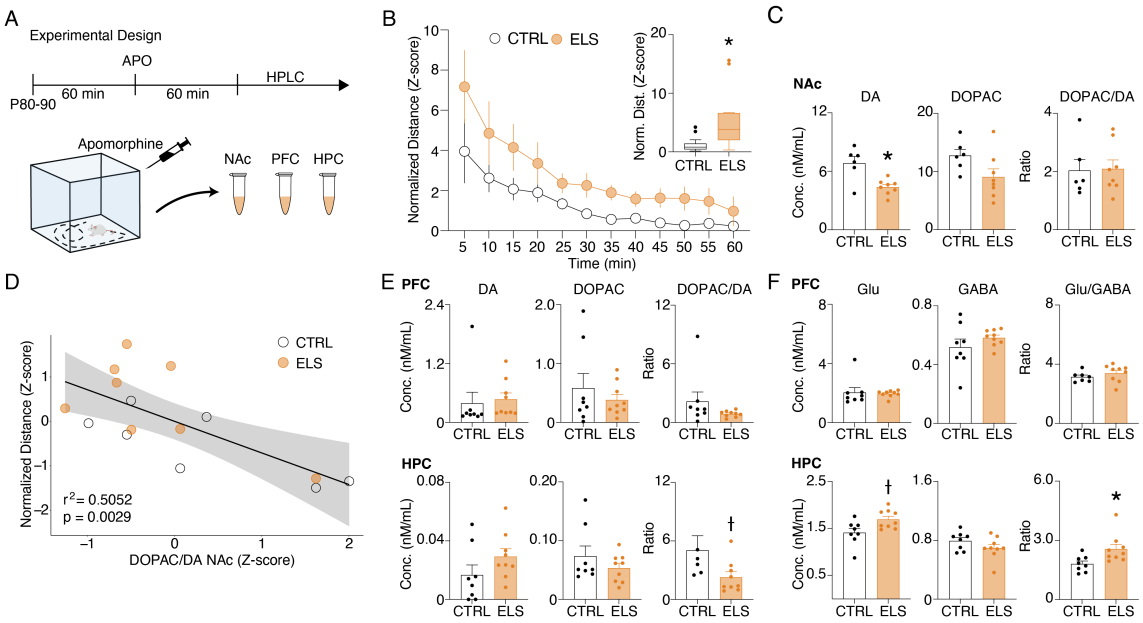

Figure 11. ELS rats present behavioral and neurochemical sensitivity to dopaminergic activation. ***A,*** Experimental design representing quantification of locomotion in the open field, apomorphine (APO) injection, and neurochemical analysis. ***B,*** Normalized locomotion across time blocks after APO injection, demonstrating increased locomotion of ELS rats induced by APO. Average normalized locomotion after APO injection (inset). ***C,*** Concentration of dopamine and metabolites in the NAc. ***D,*** GLM for the total distance after APO indicating DOPAC/DA ratio in the NAc as a strong significant variable associated with behavioral sensitivity to APO. ***E,*** Concentration of dopamine and metabolites (left) in the PFC (upper panel) and HPC (lower panel). Concentration of glutamate and GABA (right) in the PFC (upper panel) and HPC (lower panel). †Uncorrected $p < 0.05$, * multiple comparison corrected $p < 0.05$. Error bars represent the mean ± SEM.

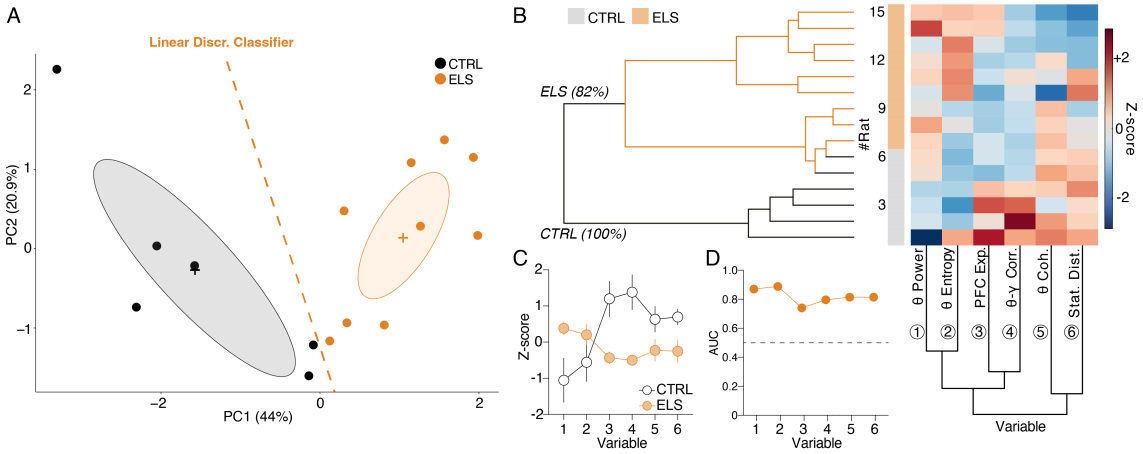

Figure 12. HPC and PFC oscillatory dynamics discriminate ELS rats. *A,* A linear discriminant classifier (dotted orange line) using the first two principal components (PCs) of relevant electrophysiological variables completely distinguishes ELS from CTRL rats (100% accuracy; 93.34% leave-one-out cross-validation). Note that the PC1 alone completely discriminates ELS rats. ***B,*** Unsupervised hierarchical clustering using the electrophysiological variables (bottom dendrogram) almost completely dissociates ELS from CTRL rats (left dendrogram). Inside the ELS cluster, we can observe one complete ELS branch, but the other overlapping with some CTRL animals, suggesting a graduality in the pathophysiological effects of ELS. ***C,*** Z-score values of each variable, showing distinct patterns of activity for each group. ***D,*** All the electrophysiological variables are good discriminators of CTRL and ELS rats (AUC-ROC > 0.7). † $p < 0.1$, *$p < 0.05$, **$p < 0.01$, ***$p < 0.001$. Error bars represent the mean ± SEM.